RESEARCH PAPER

BJP | BRITISH PHARMACOLOGICAL SOCIETY

Δ⁹-Tetrahydrocannabinolic acid alleviates collagen-induced arthritis: Role of PPARγ and CB₁ receptors

Belén Palomares[1,2,3] | Martín Garrido-Rodriguez[1,2,3] |
Claudia Gonzalo-Consuegra[4,5,6] | María Gómez-Cañas[4,5,6] | Suwipa Saen-oon[7] |
Robert Soliva[7] | Juan A. Collado[8] | Javier Fernández-Ruiz[4,5,6] |
Gaetano Morello[9] | Marco A. Calzado[1,2,3] | Giovanni Appendino[10] |
Eduardo Muñoz[1,2,3]

[1]Maimonides Biomedical Research Institute of Córdoba, University of Córdoba, Córdoba, Spain

[2]Department of Cellular Biology, Physiology and Immunology, University of Córdoba, Córdoba, Spain

[3]Reina Sofía University Hospital, Córdoba, Spain

[4]Instituto Universitario de Investigación en Neuroquímica, Departamento de Bioquímica y Biología Molecular, Facultad de Medicina, Universidad Complutense, Madrid, Spain

[5]Centro de Investigación Biomédica en Red de Enfermedades Neurodegenerativas (CIBERNED), Madrid, Spain

[6]Instituto Ramón y Cajal de Investigación Sanitaria (IRYCIS), Madrid, Spain

[7]Nostrum Biodiscovery, Barcelona, Spain

[8]Emerald Health Biotechnology, Córdoba, Spain

[9]Emerald Health Natural, Vancouver, British Columbia, Canada

[10]Dipartimento di Scienze del Farmaco, Università del Piemonte Orientale, Novara, Italy

Correspondence
Eduardo Muñoz, Maimonides Biomedical Research Institute of Córdoba, University of Córdoba, Avda Menéndez Pidal s/n, 14004 Córdoba, Spain.
Email: fi1muble@uco.es

Background and Purpose: Δ⁹-Tetrahydrocannabinolic acid (Δ⁹-THCA-A), the precursor of Δ⁹-THC, is a non-psychotropic phytocannabinoid that shows PPARγ agonist activity. Here, we investigated the ability of Δ⁹-THCA-A to modulate the classic cannabinoid CB₁ and CB₂ receptors and evaluated its anti-arthritis activity in vitro and in vivo.

Experimental Approach: Cannabinoid receptors binding and intrinsic activity, as well as their downstream signalling, were analysed in vitro and in silico. The anti-arthritis properties of Δ⁹-THCA-A were studied in human chondrocytes and in the murine model of collagen-induced arthritis (CIA). Plasma disease biomarkers were identified by LC-MS/MS based on proteomic and ELISA assays.

Key Results: Functional and docking analyses showed that Δ⁹-THCA-A can act as an orthosteric CB₁ receptor agonist and also as a positive allosteric modulator in the presence of CP-55,940. Also, Δ⁹-THCA-A seemed to be an inverse agonist for CB₂ receptors. In vivo, Δ⁹-THCA-A reduced arthritis in CIA mice, preventing the infiltration of inflammatory cells, synovium hyperplasia, and cartilage damage. Furthermore, Δ⁹-THCA-A inhibited expression of inflammatory and catabolic genes on knee joints.

The anti-arthritic effect of Δ^9-THCA-A was blocked by either SR141716 or T0070907. Analysis of plasma biomarkers, and determination of cytokines and anti-collagen antibodies confirmed that Δ^9-THCA-A mediated its activity mainly through PPARγ and CB$_1$ receptor pathways.

Conclusion and Implications: Δ^9-THCA-A modulates CB$_1$ receptors through the orthosteric and allosteric binding sites. In addition, Δ^9-THCA-A exerts anti-arthritis activity through CB$_1$ receptors and PPARγ pathways, highlighting its potential for the treatment of chronic inflammatory diseases such as rheumatoid arthritis.

1 | INTRODUCTION

The medical use of *Cannabis sativa* is centuries old, and modern studies support the potential efficacy of some phytocannabinoids in different medical conditions (Goncalves et al., 2019). Around 150 cannabinoids have been identified in different strains of Cannabis (Hanus, Meyer, Munoz, Taglialatela-Scafati, & Appendino, 2016) with Δ^9-tetrahydrocannabinol (Δ^9-THC) and cannabidiol (CBD) being the best investigated cannabinoids. These neutral cannabinoids are produced and stored in the plant as acidic precursors (cannabinoid acids) that are decarboxylated under different conditions including heating (Krejci, Horak, & Santavy, 1959; Wang et al., 2016). Remarkably, the acidic precursor of Δ^9-THC (Δ^9-THCA-A) is not psychotropic, and its binding to cannabinoid receptors is still debated (McPartland et al., 2017; Moreno-Sanz, 2016). Nevertheless, Δ^9-THCA-A is anti-emetic in shrews and this activity was reversed by co-treatment with SR141716, a selective cannabinoid CB$_1$ receptor antagonist (Rock, Kopstick, Limebeer, & Parker, 2013). In addition, we recently showed that Δ^9-THCA-A is a potent activator of PPARγ, endowed with remarkable biological activities (Nadal et al., 2017; Palomares et al., 2019).

Rheumatoid arthritis (RA) is a chronic inflammatory autoimmune disease characterized by a persistent synovial inflammation as result of a synovial hyperplasia, an increase of proinflammatory cytokines and MMPs, infiltration of inflammatory cells, and production of autoantibodies (McInnes & Schett, 2011). This inflammation also affects bone and cartilage, finishing in joint destruction (Gui, Tong, Qu, Mao, & Dai, 2015). Current medications for RA include nonsteroidal anti-inflammatory drugs, corticosteroids, and disease-modifying antirheumatic drugs. However, additional drug candidates with a good safety profile are still needed (Guo et al., 2018). Anecdotal and preclinical evidence has supported the use of cannabinoids for the treatment of arthritis, being beneficial in decreasing pain and inflammation (Bruni et al., 2018). The presence of elevated levels of the endocannabinoids N-arachidonoyl ethanolamine (AEA; anandamide) and 2-arachidonoylglycerol (2-AG), without enhanced expression of CB$_1$ and CB$_2$ receptors, has been found in synovial tissues of RA patients but not in control patients (Richardson et al., 2008). Hence, the endocannabinoid system (ECS) could represent a potential therapeutic target for RA treatment by increasing the levels of endogenous cannabinoids or modulating the activity of

What is already known

- Δ^9-THCA-A, the natural precursor of Δ^9-THC, is a major non-psychotropic phytocannabinoid present in *Cannabis sativa*.
- Δ^9-THCA-A is a potent activator of PPARγ, with anti-inflammatory and neuroprotective activity.

What this study adds

- Δ^9-THCA-A binds to CB$_1$ receptors as an orthosteric agonist and as a positive allosteric modulator.
- Δ^9-THCA-A alleviated collagen-induced arthritis in mice, through CB$_1$ receptor and PPARγ pathways.

What is the clinical significance

- Our results add additional evidence of the therapeutic potential of non-psychotropic cannabinoids.

CB$_1$ and CB$_2$ receptors (Gui et al., 2015). Notably, the use of allosteric ligands for cannabinoid receptors offers a potential opportunity as therapeutic agents. In this context, the positive allosteric modulators (PAMs) of the CB$_1$ receptor produce analgesia and attenuate neuropathic pain, without cannabimimetic side effects (Ignatowska-Jankowska et al., 2015; Slivicki et al., 2018). Indeed, there is evidence that both antagonists and agonists of CB$_1$ receptors can be useful in the modulation of arthritis (Lowin & Straub, 2015). Interestingly, activation of CB$_1$ receptors induces osteoblast activity, inhibiting bone resorption, a frequent event in arthritis (Tam et al., 2008). In addition, agonists of CB$_1$ receptors have anti-inflammatory effects on immune cells, being involved in the inhibition of T cell signalling (Kraus, 2012).

The nuclear hormone receptor PPARγ functions as a ligand-inducible transcription factor playing a key role in the regulation of lipid and glucose metabolism, but currently, it is also well known for being involved in inflammatory and immunomodulatory processes

(Szanto & Nagy, 2008). In fact, recent studies have reported that PPARγ is involved in rheumatic diseases (Fahmi, Martel-Pelletier, Pelletier, & Kapoor, 2011; Koufany et al., 2013; Marder et al., 2013). In addition, preclinical evidence suggests that PPARγ agonists exert protective effects in experimental models of arthritis, reducing disease severity, infiltration of inflammatory cells, and plasma proinflammatory cytokine levels, and preventing cartilage and bone loss (Fahmi et al., 2011). Also, some clinical trials have demonstrated that PPARγ ligand activators alleviate the symptomatology in RA patients (Marder et al., 2013; Ormseth et al., 2013).

Here, we have shown that Δ^9-THCA-A has anti-arthritic activity by targeting PPARγ and CB_1 receptor signalling pathways, highlighting its potential for the treatment of chronic inflammatory diseases including RA.

2 | METHODS

2.1 | Cell cultures

HEK293-CB_1-CRE-Luc cells were obtained from innoHealth Group S.L. (RRID:CVCL_YI92; Madrid, Spain) and HEK293 from ATCC (RRID:CVCL_0045; Manassas, VA, USA). Both were cultured in DMEM, containing 20-mM L-glutamine and supplemented with 10% FBS and antibiotics. HEK293-CB_1-β-arrestin Nomad cells were purchased from Innoprot S.L. (RRID:CVCL_YI91; Derio, Bizkaia, Spain) and cultured in DMEM supplemented with 10% FBS, 20-mM L-glutamine, puromycin (5 μg·ml^{-1}), hygromycin (80 μg·ml^{-1}), and G418 (250 μg·ml^{-1}). This cell line stably co-expresses CB_1 receptors and β-arrestin. Based on Nomad Biosensor technology, the cell line was created to identify β-arrestin recruitment following CB_1 receptor activation. To accomplish this, β-arrestin was coupled to reporters engineered with a single fluorescence protein that transduce the signal upon ligand binding to CB_1 receptors (Mella et al., 2018). Thus, in HEK293-CB_1-β-arrestin Nomad cells, the green β-arrestin biosensor become fluorescent upon activation of CB_1 receptors. All the cells were maintained at 37°C in a humidified atmosphere containing 5% CO_2.

2.2 | CB_1 and CB_2 receptor binding assay

The receptor binding of Δ^9-THCA-A (10^{-11}–10^{-4} M) was investigated by competition studies against [^{3}H]CP-55,940 to determine its binding affinity (Ki value) at both cannabinoid receptors using commercially available membranes prepared from HEK-293 cells, stably transfected with CB_1 or CB_2 receptors (RBHCB1M400UA and RBXCB2M400UA, respectively; Perkin Elmer) (Gomez-Canas et al., 2016). Briefly, membranes were added in assay buffer (for CB_1: 50-mM Tris-Cl, 5-mM MgCl$_2$.H$_2$O, 2.5-mM EDTA, 0.5 mg·ml^{-1} of BSA, pH 7.4, or for CB_2: 50-mM Tris-Cl, 5-mM MgCl$_2$.H$_2$O, 2.5-mM EGTA, 1 mg·ml^{-1} of BSA, pH 7.5) at a final concentration of 8 and 4 μg per well for CB_1 and CB_2 receptors, respectively. The radioligand

was used at 0.4 nM for CB_1 receptors or 0.53 nM for CB_2 receptors and in a final volume of 200 μl for both receptors. The reaction was stirred for 90 min at 30°C. Non-specific binding was determined with non-radiolabelled WIN55,212-2 (10 μM) in the presence of radioligand; 100% binding of the [^{3}H]CP-55,940 was determined by incubation of the membranes with radioligand in the absence of Δ^9-THCA-A. All of the plastic material employed were siliconized with Sigmacote (Sigma-Aldrich) to prevent possible adhesion of compounds. After incubation, free radioligand was separated from bound radioligand by filtration in GF/C filters, previously treated with a 0.05% (v·v^{-1}) polyethylethylenimine solution. Then filters were washed nine times with cold assay buffer, using the Harvester® filtermate equipment (Perkin Elmer). Radioactivity was measured using a liquid scintillation spectrometer (Microbeta Trilux 1450 LSC & Luminescence Counter [Perkin Elmer]). Data were expressed as percentage of [^{3}H]CP-55,940 binding.

2.3 | [^{35}S]-GTPγS binding analysis

The intrinsic activity of Δ^9-THCA-A at the cannabinoid receptors was analysed using a [^{35}S]-GTPγS binding assay with increasing concentrations (10^{-11}–10^{-4} M) of this compound (Gomez-Canas et al., 2016). The assay buffer was prepared by adding 10-μM GDP (Sigma-Aldrich) to 20-mM HEPES (Sigma-Aldrich) buffer containing 100-mM NaCl and 10-mM MgCl$_2$ at pH 7.4. Later, the radiolabelled, non-hydrolysable G-protein-activating analogue of GTP, [^{35}S]-GTPγS (Perkin Elmer), was added at a final concentration of 0.3 nM in assay buffer. The assay started once membranes (previously permeabilized with 5 μg of saponin; Sigma-Aldrich) containing CB_1 (HTSO19M) or CB_2 receptors (HTS020M) (5 μg per well; Eurofins Discovery Services, Saint Charles, MO, USA) were added. The reaction had a final volume of 100 μl and was stirred for 30 min at 30°C. To determine the non-specific signal, 10-μM GTPγS (Sigma-Aldrich) was employed. Again, 96-well plates and the tubes needed for the experiment were siliconized with Sigmacote (Sigma-Aldrich). The reaction was terminated by rapid vacuum filtration with a Harvester® filtermate equipment (Perkin Elmer) through Filtermat A GF/C filters. The filters were washed nine times with ice-cold filtration buffer (10-mM sodium phosphate, pH 7.4), and bound radioactivity was measured with a 1450 LSC & Luminiscence counter Wallac MicroBeta TriLux (Perkin Elmer).

2.4 | Analysis of allosteric properties of Δ^9-THCA-A at the CB_1 receptor

For the study of allosteric properties of Δ^9-THCA-A at the CB_1 receptor, the activation of this receptor elicited by increasing concentrations (10^{-11}–10^{-4} M) of CP-55,940 was quantified alone or in the presence of Δ^9-THCA-A at three concentrations (10^{-6}, 10^{-10}, and 10^{-13} M) following a modification of the procedure for [^{35}S]-GTPγS binding.

2.5 | CB$_1$ receptor functional assays (cAMP-arrestin and proliferation)

To study CB$_1$ receptor-mediated functional activities, HEK293-CB$_1$-CRE-Luc (5×10^4) cells were seeded in 96-well plates. After stimulation for 6 h, the cells were washed twice with PBS and lysed in 50-μl lysis buffer containing 25-mM Tris-phosphate (pH 7.8), 8-mM MgCl$_2$, 1-mM DTT, 1% Triton X-100, and 7% glycerol during 15 min at room temperature in a horizontal shaker. Luciferase activity was measured using a TriStar^2 Berthold/LB942 multimode reader (Berthold Technologies, Oak Ride, TN, USA) following the instructions of the luciferase assay kit (Promega, Madison, WI, USA). Results were represented as the percentage of activation versus control non-stimulated cells. To analyse β-arrestin recruitment, HEK293-CB$_1$-β-arrestin Nomad (1×10^4) cells were cultured in 96-well plates. The next day, the cells were stimulated as indicated, and fluorescence was measured at 0, 18, and 24 h using Live Content Cell Imaging System IncuCyte HD (Sartorius, Göttingen, DE). Cells confluence as a tool to measure proliferation was determined by IncuCyte HD Confluence Processing analysis tool.

2.6 | Docking analysis

Three available structures of the CB$_1$ receptor in an active-agonist bound state were used to prepare a grid for receptor docking: an X-ray structure (PDB code 5XR8) of CB$_1$ receptors in complex with tricyclic compound AM841 (Hua et al., 2017), a cryo-EM structure (PDB code 6N4B) of the receptors in complex with an indazole derivative (Krishna Kumar et al., 2019), and an X-ray structure (PDB code 6KQI) of the receptors in complex with CP-55,940 in the orthosteric site and the negative allosteric modulator (NAM) OR275569 bound to an extrahelical pocket overlapping with the cholesterol interaction site (Shao et al., 2019). All docking calculations on the CB$_1$ receptor structures were carried out with Schrodinger's GLIDE 2019-2 (Glide, RRID: SCR_000187) using its Standard Precision (SP) (Friesner et al., 2004) scoring and rescoring function with the extra precision (XP) (Friesner et al., 2006) scoring function. The ligand molecules were first processed with Schrodinger's Ligprep (protonation state at pH 7.4 ± 0.5) to generate 3D energy-minimized molecular structures with correct tautomeric and ionization states. The receptor grid was centred on the agonist bound orthosteric site in docking attempts to predict ligand-binding modes. Results were assessed by examining the 10 best energy poses in terms of the docking glidescore.

Protein Energy Landscape Exploration (PELE) is a highly efficient Monte Carlo (MC) algorithm that has been shown to perform extremely well at reproducing experimental binding modes in cross-docking scenarios (Grebner et al., 2017; Lecina, Gilabert, & Guallar, 2017). The basic algorithm works as follows: each MC move consists of three main steps: (i) ligand and protein perturbation; (ii) side chain rotamer sampling; and (iii) system minimization. The ligand is perturbed in a series of rotations and translations with a set of user-defined variables, whereas the protein is perturbed based on

a minimization with constrained displacements along the Cα-atoms following a set of given modes which can derive from an anisotropic network model (ANM) (Atilgan et al., 2001) or from a principal component analysis (PCA) (Lecina et al., 2017). The resulting structure obtained in the final minimization step is accepted or rejected by applying a Metropolis criterion. Backbone movements were performed by displacing backbone atoms along the first six ANM modes. This was accomplished by performing an all-atom geometry optimization, where a constraint was added to each α carbon along a randomly chosen mode (with displacements of 1.0 Å). Finally, a relaxation was accomplished with a 10° resolution side chain sampling for those residues within a distance of 4 Å to any ligand atom. In all calculations, PELE used the all atom OPLS2005 force field (Jorgensen, 1998) with an OBC implicit solvent model (Onufriev, Bashford, & Case, 2004) for protein and ligands. Interaction energies referred to in Section 3 are defined by E(AB) − E(A) − E(B), where AB stands for the complex, A for the receptor, and B the ligand. Two different PELE protocols were applied depending on the specific purpose: PELE-induced fit docking: This protocol was applied to improve the binding modes predicted from GLIDE rigid (receptor) docking for the THC series to the cryo-EM structure (PDB 6N4B). Ligand perturbation was switched between the low and medium range rotations and translations (0–15° and 0.5–1.5 Å, respectively) and only allowed to explore the area around the orthosteric binding site. A total of 1,000 PELE step simulations were run on 240 processors for 18–24 h. PELE global search: This protocol performed a dynamic exploration over the whole surface of the CB$_1$ receptor in order to locate any possible binding sites for Δ^9-THCA-A once its orthosteric site was occupied by an agonist. This protocol was performed with 40 initial positions of the ligand randomly placed around the entire protein surface (extracellular, intracellular, and membrane exposed). Since the binding site was assumed to be unknown, large rotations and translations were applied to the ligand at high SASA values and were gradually decreased at lower values of SASA (as the molecule gains more and more contacts with the receptor, translations and rotations are smaller). The simulation was run for a total of 1,000 MC steps on 240 processors for 20 h; results were analysed by inspecting the lowest interaction energy poses.

2.7 | Collagen-induced arthritis model, drug administration, and clinical evaluation

All animal care and experimental procedures were performed in accordance with European Union guideline and approved by the Animal Research Ethic Committee of Córdoba University (2018PI/18). Animal studies are reported in compliance with the ARRIVE guidelines (Kilkenny, Browne, Cuthill, Emerson, & Altman, 2010) and with the recommendations made by the British Journal of Pharmacology.

Seven-week-old male DBA/1 mice (RRID:MGI:6430738) weighing between 18 and 20 g were purchased from Janvier Labs (Le Genest Saint Isle, France). Male mice were used in the study because female mice are more resistant to develop collagen-

induced arthritis (CIA) (Holmdahl, Jansson, Larsson, Rubin, & Klareskog, 1986). The mice were housed in cages at controlled temperature ($20 \pm 2°C$) and relative humidity (40%–50%), with alternating 12-h light–dark cycles.

On day 0, mice received a first immunization, injecting 100 μl of type II bovine collagen (2 mg·ml^{-1}) (Sigma-Aldrich) emulsified in equal volumes of Freund's complete adjuvant (Sigma-Aldrich) by intradermal administration at the base of the tail. On day 21, the mice were given a booster immunization with 100 μl of type II bovine collagen (2 mg·ml^{-1}) emulsified in equal volumes of Freund's incomplete adjuvant. Following the second immunization, mice without evident symptoms were randomly assigned in different groups ($n = 9$ per group) and treated daily by i.p. injection with Δ^9-THCA-A (20 mg·kg^{-1}), with or without the selective PPARγ inhibitor, T0070907 (5 mg·kg^{-1}), the CB_1 receptor antagonist, SR141716 (3 mg·kg^{-1}), or the vehicle (ethanol/cremophor/saline in the proportion of 1:1:18) until day 36. Body weight (BW) change was monitored every 2–3 days during treatment period. The paw oedema was monitored using a Vernier calliper and a plethysmometer (LE7500, Panlab, Barcelona, Spain) at the same time. The clinical evaluation of arthritis severity was scored on a scale of 0 to 4 for each whole mouse as follows: 0 = normal; 1 = detectable swelling in one joint or toe; 2 = swelling in two types of toes or joints but not entire paw inflamed; 3 = entire paw inflamed and swollen; and 4 = severe swelling in the entire paw or ankylosed. At the end of the treatment period, mice were killed, and blood and hind limb tissue were collected for analysis. Tissues were immediately frozen using dry ice and then stored at $-80°C$ and/or fixed by immersion in a 4% formalin solution for further analysis of molecular expression and histology, respectively. Blood was collected into heparin tubes and centrifuged at 1500 x g for 20 min at $4°C$.

In a separate set of experiments, we tested the hypolocomotion and catalepsy effects of both Δ^9-THC and Δ^9-THCA-A at 20 mg·kg^{-1} during 30 min in control mice (Videos S1 and S2) and evaluated the effects of T0070907 (5 mg·kg^{-1}) and SR171416 (3 mg·kg^{-1}) individually in CIA mice (Figures S2 and S3).

2.8 | Histological evaluation of arthritis

The knee joint of each mouse was isolated and fixed in 4% formalin for 2 days and decalcified in 7% nitric acid for 5 days. After decalcification, samples were processed and embedded in paraffin. Sagittal sections were stained with haematoxylin and eosin (H&E), safranin O, and toluidine blue. The degree of inflammation was examined based on H&E staining according to the following scheme: 0, normal knee joint; 1, normal synovium with occasional mononuclear cells; 2, definite arthritis, a few layers of flat to rounded synovial lining cells and scattered mononuclear cells; 3, clear hyperplasia of the synovium with three or more layers of loosely arranged lining cells and dense infiltration with mononuclear cells; and 4, severe synovitis with pannus and erosions of articular cartilage and subchondral bone. Based on safranin O and toluidine blue staining, a score was assigned to describe the cartilage damage: 0, no destruction; 1, minimal erosion, limited to

single spots; 2, slight to moderate erosion in a limited area; 3, more extensive erosion; and 4, general destruction. Pictures were taken using a Leica DM2000 microscope and Leica MC190 camera.

2.9 | Real-time PCR

The knee joints from mice were dissected after 2 weeks on treatment, and total RNA was extracted using QIAzol Lysis Reagent (Qiagen, Hilden, Germany) and purified with RNeasy Mini Kit (Qiagen). cDNA was synthesized using the iScript™ cDNA Synthesis Kit (Bio-Rad, Hercules, CA, USA). A CFX96 Real-Time PCR Detection System (Bio-Rad) was used for PCR amplification. All reactions were performed using the iQTM SYBR Green Supermix (Bio-Rad). Gene expression was standardized to GADPH mRNA levels in each sample. The primer sequences for the quantitative real-time PCR are shown in Table S1.

2.10 | Quantification of cytokines and autoantibodies

Cytokine levels (IFN-γ, IL-6, IL-10, IL-17A, and TNF-α) and IgG antibody levels against type II collagen were measured in plasma using quantitative Bio-Plex Pro™ Mouse Cytokine Th17 Panel A 6-Plex immunoassay (Bio-Rad, Cat# M6000007NY, RRID:AB_2784537) and Mouse Anti-Type II Collagen IgG Assay Kit (Chondrex, Redmond, WA, USA, Cat# 2036T, RRID:AB_2848198) according to the manufacturer's protocols, respectively.

2.11 | Western blots

HEK293-CB_1-β-arrestin Nomad and HEK293 cells (3.5×10^5) were seeded in six-well plates. The next day, the cells were deprived of serum (1% FBS) for 18 h, after which they were pre-incubated with SR141716 for 5 min and then treated with Δ^9-THCA-A and CP-55,940 for 25 min. Proteins were isolated with NP-40 lysis buffer (50-mM Tris–HCl pH 7.5, 150-mM NaCl, 10% glycerol, and 1% NP-40) supplemented with 10-mM NaF, 1-mM Na_3VO_4, 10 μg·ml^{-1} of leupeptin, 1 μg·ml^{-1} of pepstatin and aprotinin, and 1 μl·ml^{-1} of PMSF. Samples (30 μg) were analysed by electrophoresis in 8% SDS-PAGE gels and transferred to PVDF membranes. The expression of phospho-ERK1/2 and total ERK1/2 was analysed, and anti-β-actin was used for loading control. Membranes were incubated with the appropriate HRP-conjugated secondary antibody and detected by chemiluminescence system (GE Healthcare Europe GmbH, Freiburg, Germany).

2.12 | Proteomic analysis

The depletion of the three most abundant proteins in plasma was performed using the Hu-7 Multiple Affinity Removal System kit (Agilent

Technologies, Wilmington, DE, USA) following the manufacturer's instructions. The remaining proteins were concentrated using 5,000 MW cut-off (MWCO) spin concentrators (Agilent Technologies); then the cells were lysed and cleaned to remove any contaminants by protein precipitation with TCA/acetone and solubilized in 50 μl of 0.2% RapiGest SF (Waters, Milford, MA, USA) in 50-mM $(NH_4)HCO_3$. The total protein was measured using the Qubit Protein Assay Kit (Thermo Fisher Scientific, Waltham, MA, USA), and 50 μg of protein from each sample was subjected to trypsin digestion. In order to build the spectral library and quantify the samples by SWATH acquisition, we followed the method previously described by Ortea, Ruiz-Sanchez, Canete, Caballero-Villarraso, and Canete (2018). Briefly, the peptide solution was analysed by a shotgun data-dependent acquisition (DDA) approach using nano-LC-MS/MS. Then the samples were pooled in five groups of six samples each, and 1 μg was separated into a nano-LC system Ekspert nLC400 (Eksigent, Dublin, CA, USA). Peptide and protein identifications were performed using Protein Pilot software v5.0 (Sciex, RRID:SCR_018681) with a human UniProtKB concatenated target-reverse decoy database, specifying iodoacetamide as alkylation. The false discovery rate (FDR) was set to 0.01 for both peptides and proteins. The MS/MS spectra of the identified peptides were used to generate the spectral library for SWATH peak extraction using the add-in for PeakView Software v2.1 (Sciex) MS/MS^{ALL} with SWATH Acquisition MicroApp v2.0 (Sciex). The normalized SWATH areas matrix was then imported into the R statistical programming environment for further analyses and visualization. Pairwise data comparisons were performed for every condition against the control by applying a Welch two-sample T-test, and resultant P values were adjusted to control the FDR. The MS proteomic data have been deposited in the ProteomeXchange Consortium via the PRIDE partner repository (Pride-asap, RRID:SCR_012052, accession no. PXD015274).

2.13 | Data and statistical analysis

The data and statistical analysis comply with the recommendations of the *British Journal of Pharmacology* on experimental design and analysis in pharmacology (Curtis et al., 2018). The animals were randomized into groups of equal size. All the treatments and experiments were blinded and analysed by different investigators. The histological images were evaluated by two independent observers. For statistical analysis, each group size was at least $n = 5$, and no outliers were excluded. Group sizes were selected, based on the results of previous comparable studies. in vitro data are expressed as mean ± SD, and in vivo and binding assays results are represented as mean ± SEM. Data that showed a normal distribution from two groups were tested using a Student's T-test. The significance between three or more independent groups was analysed using one-way ANOVA followed by Tukey's post hoc test. The data that involved two independent variables were tested using a two-way ANOVA followed by a Bonferroni multiple comparison test. Data not normally distributed were analysed by the Kruskal–Wallis followed by Dunn's post hoc test. Post hoc

analyses in ANOVA tests were carried out when F achieved was $P < 0.05$, and there was no significant variance in homogeneity. The value of $P < 0.05$ was considered significant. N values were derived from independent animals or experiments, not replicates. Some results were normalized to minimize variations between independent experiments. Statistical analysis was performed using GraphPad Prism® version 6.01–7 (GraphPad Prism, RRID:SCR_002798).

2.14 | Materials

The isolation of Δ^9-THCA-A followed the method of Krejci and Santavy (1955) for the isolation of acidic cannabinoids from plant sources. The plant material (50 g; powdered flowerheads of a mixture of various chemotypes of *C. sativa* generated during breeding experiments at CRA) was supplied by Dr. Gianpaolo Grassi, CRA Rovigo (Italy). Ministry of Health, under Contract # SP/041 of 10/03/2016 to Università del Piemonte Orientale. This starting material contained 8% Δ^9-THC, assayed by GC. The powdered material was extracted with acetone. After removal of the solvent, the residue (12.6 g) was partitioned between petroleum ether (250 ml) and 2% NaOH (3 × 100 ml). The pooled basic solutions were washed with petroleum ether (100 ml), cooled in an ice bath, and acidified to pH 3 with the cautious dropwise addition of concentrated H_2SO_4. A gummy material separated and the heterogeneous mixture were extracted with $CHCl_3$ (2 × 80 ml). The pooled organic phases were washed with brine and evaporated. The residue (4.3 g) was purified by gravity column chromatography on silica gel (100 g, petroleum ether–EtOAc gradient). The fractions eluted with petroleum ether:EtOAc, 4:6 were evaporated and crystallized from ether to afford Δ^9-THCA-A (1.3 g) as an off-white powder. This final product was >97% pure by HPLC analysis and its identity confirmed by ^{1}H and ^{13}C NMR (Choi et al., 2004), against a standard sample used previously (Cuadari et al., 2019; Nadal et al. 2017).

HEPES, GDP, PD98059, T0070907, WIN55,212-2 and CP-55,940 were purchased from Sigma-Aldrich (St. Louis, MO, USA), and SR141716 was purchased from Tocris Bioscience (Bristol, UK). [^{3}H] CP-55,940 (164.5 Ci·mmol^{-1}) was supplied by Perkin Elmer, Boston, MA, USA. Antibodies used in this study are as follows: anti-phospho-ERK1/2 (Cell Signaling Technology, Danvers, MA, USA, Cat# 9101, 1:2,000, RRID:AB_331646), anti-MAPK (ERK1/2) (Sigma-Aldrich, Cat# M5670, 1:10,000, RRID:AB_477216), and anti-β-actin (Abcam, Cambridge, UK, Cat# 40900, 1:50,000, RRID:AB_867494).

2.15 | Nomenclature of targets and ligands

Key protein targets and ligands in this article are hyperlinked to corresponding entries in http://www.guidetopharmacology.org, the common portal for data from the IUPHAR/BPS Guide to PHARMACOLOGY (Harding et al., 2018), and are permanently archived in the Concise Guide to PHARMACOLOGY 2019/20 (Alexander, Christopoulos et al., 2019; Alexander, Cidlowski et al., 2019; Alexander, Fabbro et al., 2019; Alexander, Kelly et al., 2019).
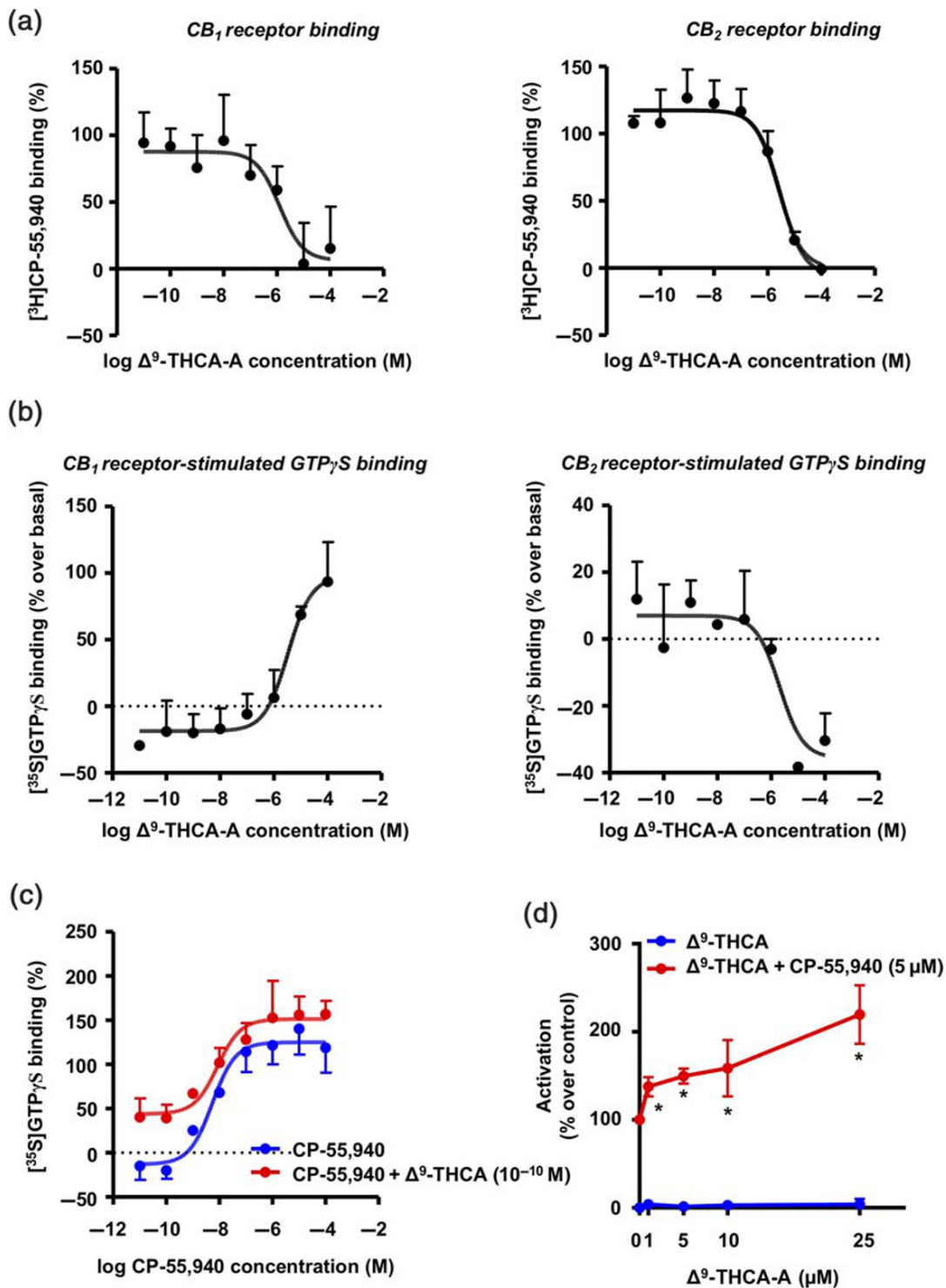
FIGURE 1 Identification of Δ^9-THCA-A as a positive allosteric modulator of CB_1 receptors. (a) Binding affinity of Δ^9-THCA-A to CB_1 and CB_2 receptors. Ki values obtained from competition studies using [^{3}H] CP-55,940 as radioligand for hCB_1 and hCB_2 receptors. (b) Average concentration–response curves for the stimulation of [^{35}S]-GTPγS binding by Δ^9-THCA-A. (c) [^{35}S]-GTPγS binding stimulated by CP-55,940 (10^{-4}–10^{-11} M) in the absence or presence of Δ^9-THCA-A (10^{-10} M). Data were expressed as mean ± SEM of five experiments performed in triplicate for each point. Ki values for each receptor and the Emax and EC_{50} (or IC_{50}) values were determined by using GraphPad Prism® version 7. (d) Receptor-specific transactivation by Δ^9-THCA-A. HEK293-CB_1-CRE-Luc cells were pre-incubated with increased concentrations of Δ^9-THCA-A for 20 min and then stimulated with CP-55,940 (5 μM) for 6 h. The values of untreated controls were taken as 100% activation ± SD ($n = 5$). $^*P < .05$, significantly different from Δ^9-THCA-A alone; two-way ANOVA followed by Bonferroni's post hoc test

3 | RESULTS

3.1 | Affinity, intrinsic activity, and potential allosteric properties of Δ^9-THCA-A at cannabinoid receptors

We first analysed Δ^9-THCA-A in competition studies to determine its affinity at CB_1 and CB_2 receptors. Δ^9-THCA-A has a modest affinity (Ki values in the submicromolar range) at both receptors, with a twofold higher affinity for **CB_1** (Ki = 252 ± 140 nM) than for CB_2 receptors (Ki = 506 ± 198 nM) (Figure 1a). Compared to a classic

ligand for both receptors such as CP-55,940, the binding of Δ^9-THCA-A to CB_1 and CB_2 receptors was more than 50-fold and 100-fold lower, respectively (Pandey, Roy, Liu, Ma, & Pettaway, 2018). The study of its intrinsic activity at the CB_1 receptor in an [^{35}S]-GTPγS binding assay showed Δ^9-THCA-A to be a partial agonist with an EC_{50} = 3.8 ± 0.5 μM (more than 100-fold higher, reflecting lower activity) compared with CP-55,940 (Pandey et al., 2018), whereas it apparently behaved as an antagonist/inverse agonist, with an IC_{50} = 1.3 ± 0.4 μM at the CB_2 receptor (Figure 1b). Lastly, we also wanted to explore whether Δ^9-THCA-A may have any allosteric activity at the CB_1 receptor. To this end, we compared the
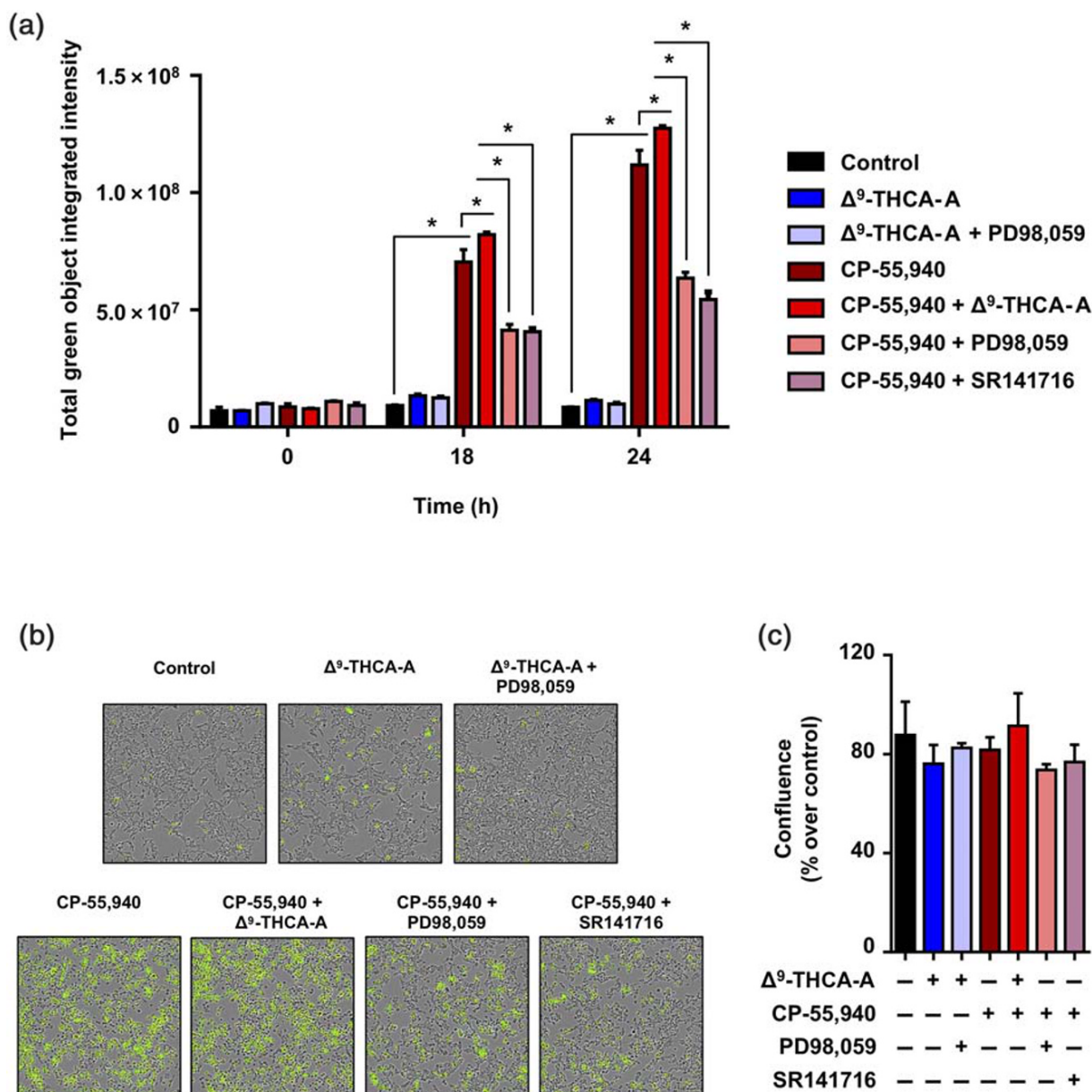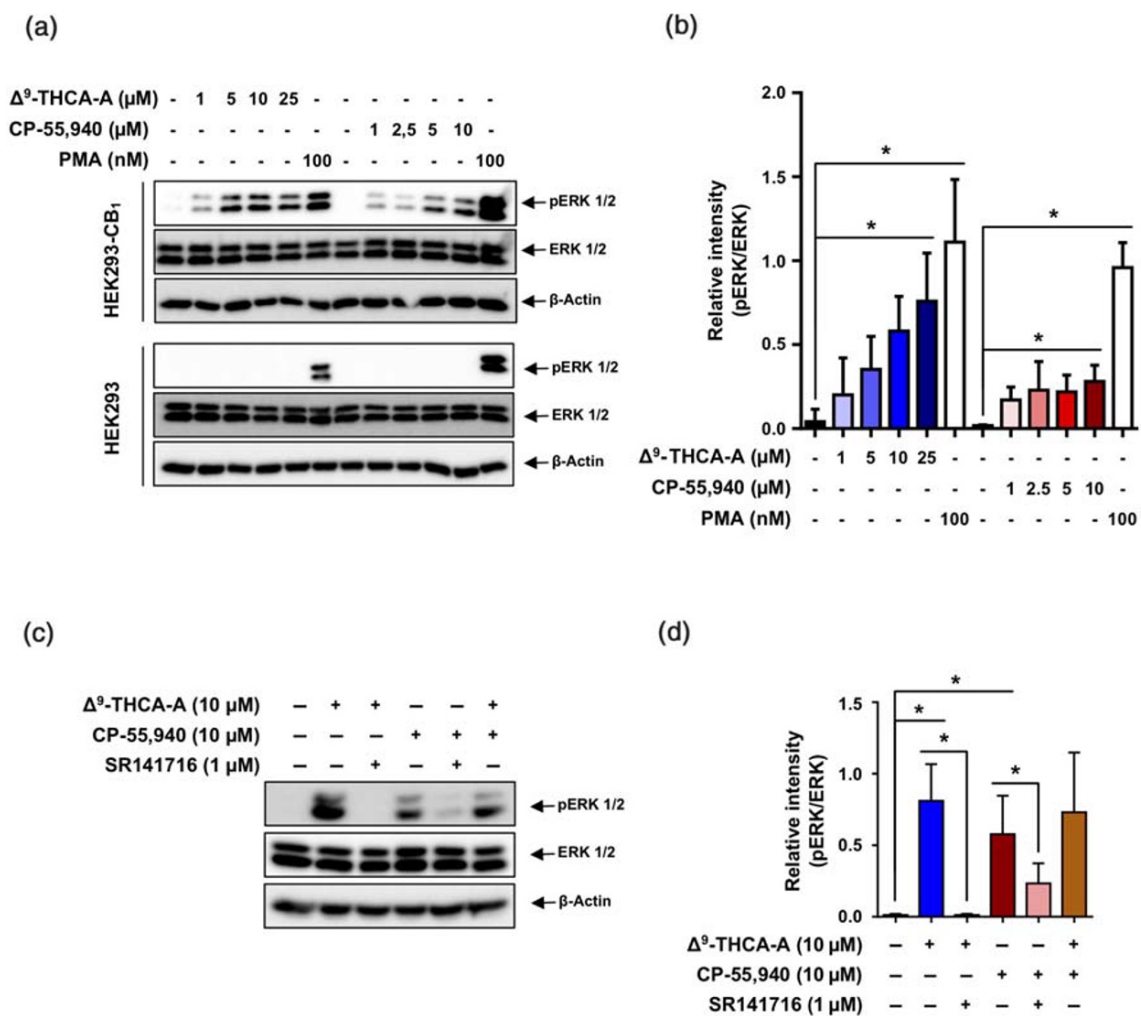

FIGURE 2 Effects of Δ^9-THCA-A on β-arrestin recruitment. HEK293-CB_1-β-arrestin Nomad cells were pre-incubated with Δ^9-THCA-A (1 μM), PD98,059 (5 μM), and SR141716 (1 μM) for 20 min and then treated with CP-55,940 (2.5 μM) for 24 h. (a) Quantification of β-arrestin recruitment on living cells at the times indicated are shown by fluorescence intensity changes. (b) Representative images of cytoplasmic fluorescence (4× magnification) and (c) cell confluence, at the endpoint were determined using the IncuCyte system. Control group was taken as 100% confluent. Data are means ± SD; n = 5. *P < .05, significantly different as indicated

activation of the CB_1 receptor in the $[^{35}S]$-GTPγS binding assay elicited by increasing concentrations of CP-55,940 in the absence or the presence of Δ^9-THCA-A at 0.1 nM, a concentration at which binding of the compound and and activation of the orthosteric site at the CB_1 receptor would be negligible, according to our competition studies (see Figure 1a). Our data indicated that, at this concentration, however, Δ^9-THCA-A significantly enhanced the CP-55,940-dependent activation of the CB_1 receptor (Figure 1c). This effect of Δ^9-THCA-A was seen at both high (Emax [% over basal] = 125.1 in the absence of Δ^9-THCA-A vs. Emax [%] = 151.5 in the presence of Δ^9-THCA-A) and low (Emin [%] = −13.1 in the absence of Δ^9-THCA-A vs. Emin [%] = 43.9 in the presence of Δ^9-THCA-A) concentrations of CP-55,940 (Figure 1c). Such enhancement was not found at a higher concentration (1 μM) at which Δ^9-THCA-A is effective at the orthosteric site (see Figure 1a), or at a lower concentration (0.1 pM) of Δ^9-THCA-A (Figure S1). However, in the case of this last concentration (0.1 pM), the values of $[^{35}S]$-GTPγS binding showed a trend towards increase when stimulated by CP-55,940 in the presence of Δ^9-THCA-A, an effect which was not statistically significant. Such trends were observed only at low concentrations of CP-55,940 (10^{-11} and 10^{-10} M) (Figure S1). In our opinion, this should progressively disappear at lower concentrations of either CP-55,940 or Δ^9-THCA-A, given the binding profiles of both cannabinoids, whereas the opposite, that this apparent increase may be enhanced reaching statistical significance when using lower concentrations, appears unlikely. In any case, we cannot exclude that the Δ^9-THC contamination in the Δ^9-THCA-A preparation is accounting for this effect and further experiments will be necessary to clarify this question.

The binding affinity of Δ^9-THCA-A for CB_1 receptor inspired us to study its effect on downstream signalling. We stimulated HEK293-CB$_1$-CRE-Luc cells with either Δ^9-THCA-A or CP-55,940

FIGURE 3 Effects of Δ^9-THCA-A on ERK1/2 phosphorylation. (a) Western blot analysis showing p-ERK1/2, total ERK1/2, and actin levels in HEK293-CB$_1$-β-arrestin Nomad cells and HEK293 cells exposed to increased concentrations of Δ^9-THCA-A and CP-55,940 for 30 min. (b) Quantification of western blot results from five independent experiments. (c) Western blot analysis in HEK293-CB$_1$-β-arrestin Nomad cells pre-stimulated with Δ^9-THCA-A (10 μM) and SR141716 (1 μM) for 5 min and treated with CP-55,940 (10 μM) for 30 min. (d) Quantification of western blot results from five independent experiments. PMA (100 nM) was used as a positive control of ERK1/2 phosphorylation. Data are means ± SD; n = 5. $^*P$ < .05, significantly different as indicated
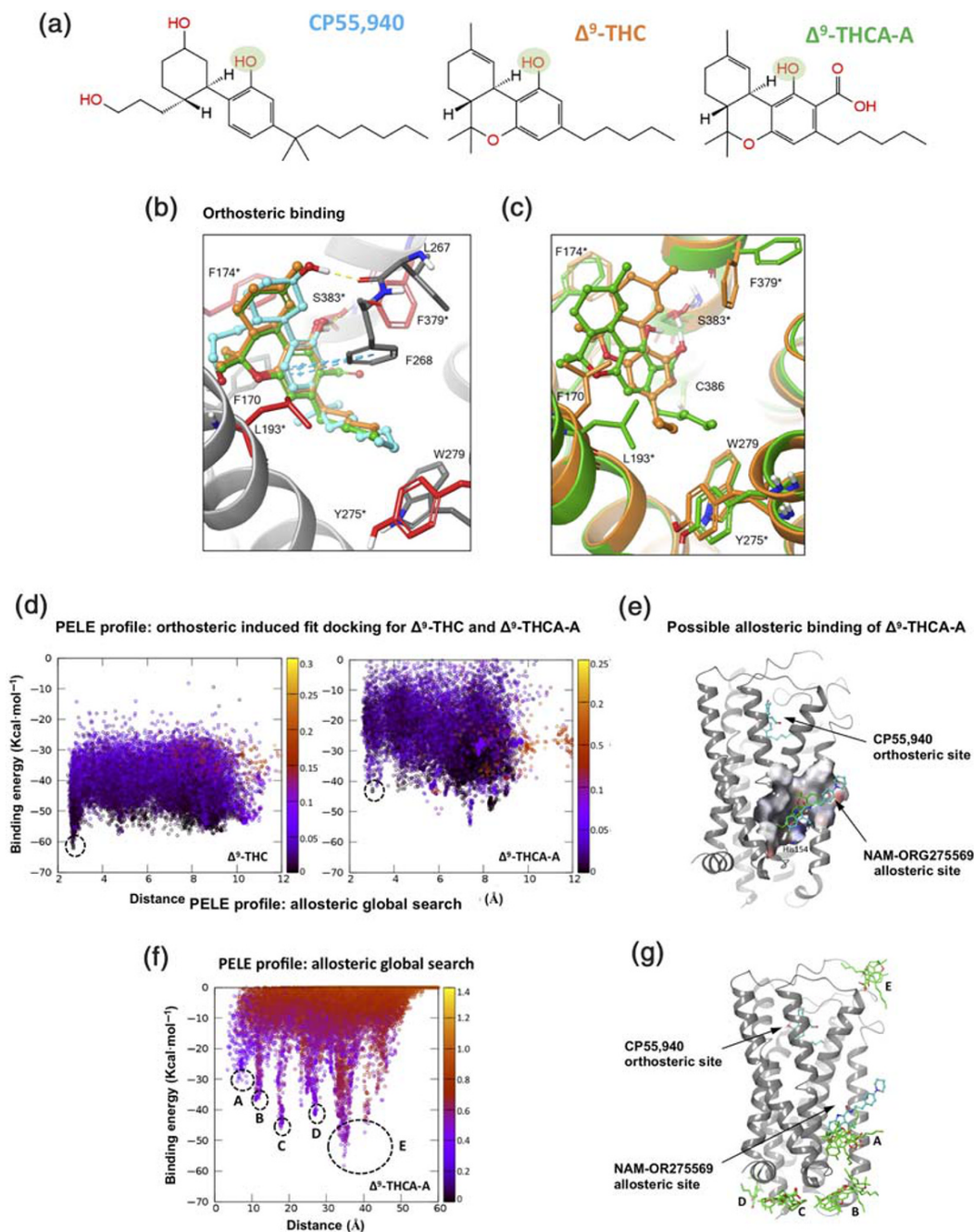
FIGURE 4 Binding mode prediction from docking and PELE simulations for three modulators of CB$_1$ receptors. (a) 2D chemical structure of compounds CP-55,940, Δ^9-THC, and Δ^9-THCA-A. A key hydroxyl functional group present in all compounds is highlighted in green. Colour coding for (a)–(c) is CP55,940, Δ^9-THC, and Δ^9-THCA-A in blue, orange, and green, respectively. *Binding mode prediction at orthosteric site*: (b) Rigid (receptor) top docking results of CP-55,940 and Δ^9-THC to the orthosteric site of CB$_1$ X-ray structure PDB 5XR8. Residues interacting with ligands are shown, and important residues identified by mutagenesis experiments are depicted in red sticks and labelled with an asterisk. (c) PELE induced-fit binding simulation results for Δ^9-THC and Δ^9-THCA-A to the CB$_1$ cryo-EM structure PDB 6N4B. *Binding mode prediction at possible allosteric site*: (d) PELE energy profiles for induced-fit docking representing interaction energy (in kcal·mol^{-1}) versus distance between the key hydroxyl group on all modulators and the sidechain OG atom of Ser383 (in Å). The black dash circles in all three plots represent the binding conformation for each molecule that best overlaps with the docking results of CP-55,940 and Δ^9-THC and the recently disclosed binding mode of CP-55,940 in the orthosteric site. (e) Rigid (receptor) top docking pose of Δ^9-THCA-A to the allosteric site of NAM-ORG275569 (represented in blue) for CB$_1$ receptor X-ray structure PDB 6KQI, where the orthosteric site is occupied by CP-55,940. The allosteric pocket is represented with molecular surface showing His154 making H-bonded interaction with carboxylate functional group of Δ^9-THCA-A (in green). (f) PELE energy profile for global search, interaction energy (in kcal·mol^{-1}) plots versus distance between the carboxylate group of Δ^9-THCA-A and the sidechain of His154 lying at the base of the NAM-ORG275569 allosteric site (in Å). The black dashed circles represent the low energy minima corresponding to the representative structures depicted in (c) and (g). (g) PELE global search simulation depicted position on the CB$_1$ receptor surface corresponding to the lowest energy poses, black dashed circles in PELE profile (f)

separately or in combination, and the luciferase activity was measured as indicative of cAMP induction. Δ^9-THCA-A did not induce CRE-Luc activity but enhanced significantly the effect of the orthosteric ligand CP-55,940 (Figure 1d). Next, we analysed whether Δ^9-THCA-A was also able to activate CB_1 receptors through β-arrestin in HEK293-CB_1-β-arrestin Nomad cells. This cell line was designed for the analysis of the receptor response that results in the activation of a green fluorescent β-arrestin Nomad biosensor, displaying an elevation in the fluorescent signal intensity of the biosensor. We found that Δ^9-THCA-A alone slightly induced β-arrestin recruitment, compared with CP-55,940, which exhibited a pronounced increase of β-arrestin recruitment (Figure 2a,b). Interestingly, Δ^9-THCA-A was able to enhance β-arrestin recruitment induced by CP-55,940, but it did not affect cell proliferation (Figure 2c). As expected, the CB_1 receptor antagonist SR141716 and the selective ERK1/2 pathway inhibitor PD98,059 decreased the β-arrestin recruitment induced by CP-55,940 (Figure 2a,b). Next, we evaluated the signalling pathway involving the phosphorylation of ERK1/2 induced by activation of CB_1 receptors. As shown in Figure 3a,b, both Δ^9-THCA-A and CP-55,940 treatments induced the phosphorylation of ERK 1/2 (pERK1/2) in a concentration-dependent manner in HEK293-CB_1 cells, but not in HEK293 cells. The induction of pERK1/2 by both Δ^9-THCA-A and CP-55,940 was inhibited by SR141716 (Figure 3c,d). Altogether, our results suggest that Δ^9-THCA-A may exert biological activities by acting as an orthosteric ligand and also as a PAM of CB_1 receptors.

3.2 | Docking

To identify the binding mode of CP-55,940, Δ^9-THC and Δ^9-THCA-A (Figure 4a) to CB_1, a set of in silico experiments were performed. Rigid (receptor) cross-docking calculations could reproduce the correct binding mode for CP-55,940 and Δ^9-THC when using the CB_1 receptor structure of PDB code 5XR8 (Figure 4b). The top docking pose for Δ^9-THC binds with the core tricyclic rings sandwiched between TM2, TM3, and TM7 in a hydrophobic pocket surrounded by residues (Figure 4b). The most critical H-bond interaction to the hydroxyl sidechain of Ser383 (TM7), with the hydroxyl moiety highlighted in Figure 4a, is preserved. Previous mutagenesis experiments identified Ser383, Phe174, Leu193, Phe379, and Tyr275 as important residues for the binding of Δ^9-THC and CP-55,940 (labelled in Figure 4b,c with an asterisk) (Hua et al., 2017; Kapur et al., 2007; Shim, Bertalovitz, & Kendall, 2011). The alkyl chain is placed perpendicular to the tricyclic core contacting Leu193, Trp279, and Tyr275, giving the molecule an "L-shaped" bioactive conformation.

Although the binding mode of CP-55,940 is similar to that of Δ^9-THC, it has an additional interaction other than the hydroxyl-Ser383 H-bond, namely, an extra H-bond to the backbone carbonyl of Leu267 (Figure 4b) through its second hydroxyl group. The stronger electrostatic interaction probably explains its higher potency. Remarkably, the predicted binding mode of CP-55,940 on PDB 5XR8 coincides perfectly with the recently published X-ray structure of CB_1 receptors

in complex with this molecule occupying the orthosteric site (PDB entry 6KQI) (Shao et al., 2019). Docking of Δ^9-THCA-A to the same X-ray CB_1 receptor structure, suggests that it shares the same binding mode with CP-55,940 and Δ^9-THC. The most important H-bond interaction to Ser383 is preserved (Figure 4b). However, the Glide XP predicted affinity is much weaker for Δ^9-THCA-A, (−8.9) than that of CP-55,940 and Δ^9-THC, probably due to the fact that its carboxylic acid does not engage the protein in any electrostatic interaction.

Our PELE-induced fit simulation for Δ^9-THC generated a lowest energy minimum binding mode that perfectly matches the docking pose and X-ray structures, placing it on the orthosteric site (Figure 4d) and recovering all key interactions (H-bond to Ser383, overall L-shape; Figure 4c, orange compound). Thus, the same PELE simulations were repeated for Δ^9-THCA-A to estimate whether it also engages the orthosteric site. However, as seen in their interaction energy plots (Figure 4d), Δ^9-THCA-A seems to engage the CB_1 receptor in the orthosteric site, as well as many other sites involving the extracellular loops with similar interaction energies. In other words, the energy profile leading to the orthosteric site is pronounced for Δ^9-THC, but not for Δ^9-THCA-A, which could have additional interaction sites involving the entrance to the orthosteric site.

The recently solved X-ray structure of CB_1 receptors in complex with agonist CP-55,940 and the NAM **ORG27569** (PDB code 6KQI) (Shao et al., 2019) revealed the allosteric modulator bound to an extrahelical site within the inner leaflet of the membrane, overlapping with a conserved cholesterol binding site seen for many GPCRs (Figure 4e). As a first attempt, tests with rigid (receptor) docking of Δ^9-THCA-A to this site predicted a binding mode that overlaps with that for ORG27569. However, the interaction is very weak, Glide XP giving a score of −5.78 kcal·mol^{-1} (Figure 4e). As a more thorough test of possible interaction sites for Δ^9-THCA-A on any pocket of the CB_1 receptor, an exhaustive global exploration with this molecule was performed on the same X-ray structure (PDB code 6KQI) with CP-55,940 occupying the orthosteric site. The energy profile for the global search is presented in Figure 4f as a plot of interaction energy versus the distance between the carboxylate group of Δ^9-THCA-A and the side chain of His154 located at the base of the allosteric pocket. The global exploration generates five energy minima (A–E), highlighting potential interaction hotspots for Δ^9-THCA-A when the orthosteric site is occupied with an agonist, in this case, CP-55,940. The structural location for each of the A–E minima on the plot is shown in Figure 4g. Inspection of these hotspots suggests that Δ^9-THCA-A could be binding on the extracellular loops, the intracellular side of the CB_1 receptor contacting G proteins, or the NAM-ORG27569/cholesterol site mentioned above.

3.3 | Δ^9-THCA-A prevents CIA-induced inflammation in vivo

It has been suggested that pharmacological manipulation of ECS as well as PPARγ agonists may represent new therapeutic options for

the management of inflammatory diseases including RA (Fahmi et al., 2011; Gui et al., 2015; Koufany et al., 2013). To study the therapeutic potential of Δ^9-THCA-A on arthritis, we used the murine CIA model (Figure 5a), which is the most widely used model for preclinical evaluation of anti-arthritis drug candidates (Seeuws et al., 2010). Induction of CIA resulted in a significant reduction in BW as well as an increase in arthritis score compared to control mice (Figure 5b,c). Treatment with Δ^9-THCA-A, starting on day 21 after induction, when the animals showed the first symptoms of arthritis, prevented weight loss (Figure 5b) and the development of severe arthritis (Figure 5c). In

addition, paw inflammation measured with a plethysmometer and a calliper at the end of treatment revealed the potent anti-inflammatory activity of Δ^9-THCA-A (Figure 5d,e), which was significantly prevented when the animals were treated with Δ^9-THCA-A in the presence of either SR141716 or T0070907. The magnitude of joint inflammation and cartilage damage were assessed by H&E and safranin O and toluidine blue staining, respectively. Knee histological analysis showed that Δ^9-THCA-A prevented the pathological manifestations of RA that includes infiltration of inflammatory cells, synovial hyperplasia, pannus (H&E staining), and articular cartilage and
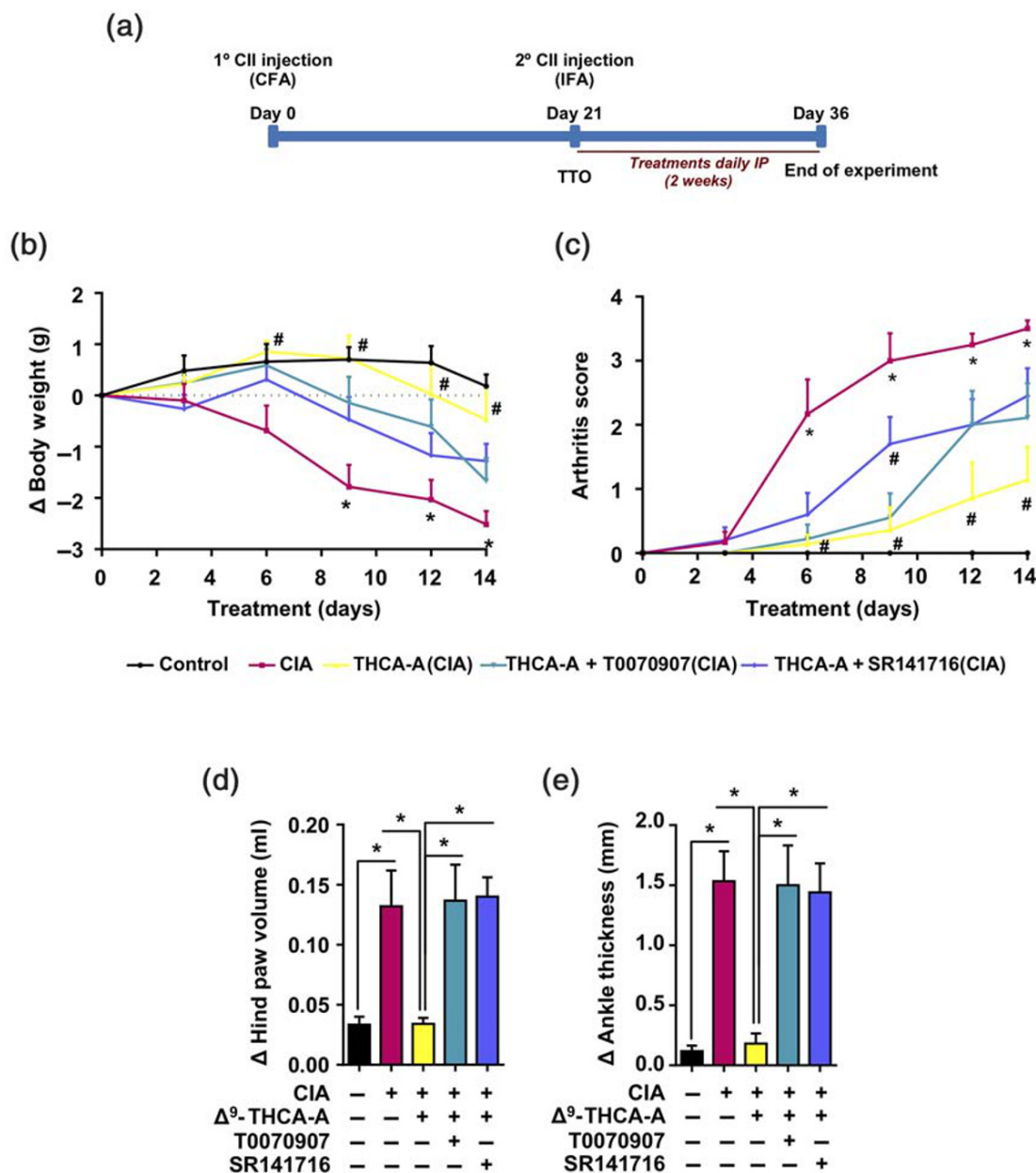

FIGURE 5 Effect of administration of Δ^9-THCA-A in a model of collagen-induced arthritis. (a) Timeline of treatment experiments in the CIA model. (b) Cumulative body weight change and (c) clinical scores in control mice, CIA-induced mice, and treated mice during the treatment; values are referenced at the beginning of treatment (taken as 0). Measurement of paw swelling using a (d) plethysmometer and (e) callipers at the end of the 2-week treatment period. Data are means ± SEM; $n = 9$ mice per group. In (b, c), $^*P < .05$, significantly differences between CIA mice and control mice; $^\#P < 0.05$, significantly differences between vehicle- or Δ^9-THCA-A + SR141716-treated CIA mice and Δ^9-THCA-A-treated CIA mice. For (d, e), $^*P < .05$, significantly different as indicated

proteoglycan loss (safranin O and toluidine blue staining), compared with the data from the untreated CIA group (Figure 6a). The score for quantification of inflammation (H&E staining) and cartilage damage (safranin O and toluidine blue staining) reflected that the treatment with Δ^9-THCA-A presented clear anti-inflammatory (Figure 6b) and chondroprotective properties (Figure 6c). Again, co-treatment with either T0070907 or SR141716 blocked the therapeutic effect of Δ^9-THCA-A. Neither T0070907 nor SR141716 separately showed significant effects on the major CIA end-points measured (Figures S2 and S3). Altogether, these results confirm that Δ^9-THCA-A is signalling through both CB$_1$ receptors and PPARγ in vivo.

Next, to determine local inflammatory and catabolic changes, mRNA levels of specific cytokines, chemokines, and immune markers (TNF-α, IL-1β, IL-6, IL-17, CXCL16, CCL2, and ICAM-1), proinflammatory mediators (COX-2 and iNOS), and catabolic markers (MMP-13 and ADAMTS5) linked to arthritis pathogenesis were assessed in the knee joints at the end of treatment. As shown in Figure 7, mRNA levels for TNF-α, IL-1β, IL-6, IL-17, CXCL16, CCL2, ICAM-1, RANKL COX-2, iNOS, and ADAMTS5 were significantly higher in the CIA group compared to control group. Moreover, levels of MMP-13 tended to increase in CIA mice. All these results were consistent with the joint damage linked to arthritis.
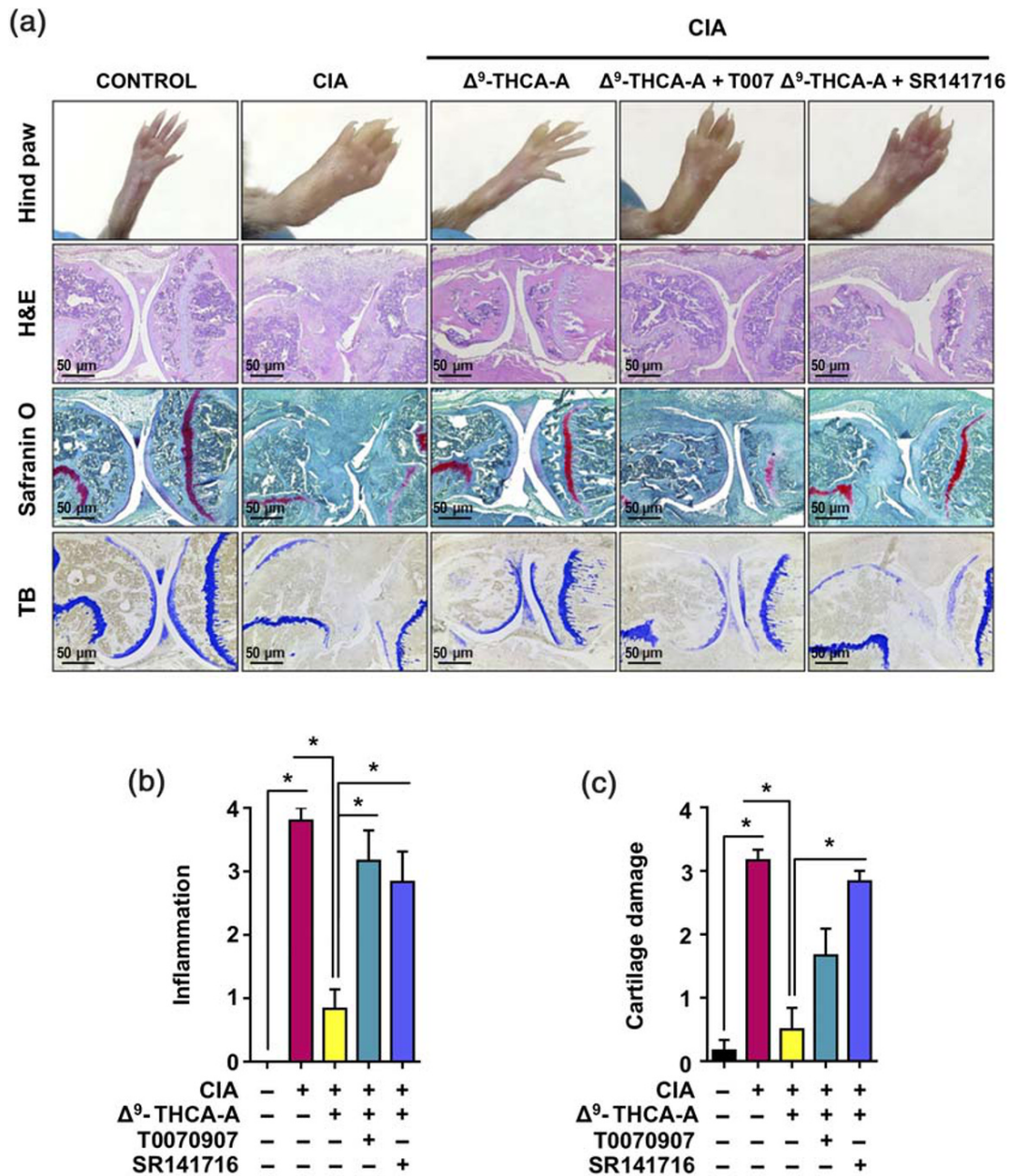
FIGURE 6 Effect of Δ^9-THCA-A on knee joints of the hind limbs in CIA mice. (a) Representative hind paw images and joint sections with haematoxylin and eosin (H&E), safranin O, and toluidine blue staining (original magnification 40×). (b) Scoring of histological inflammation was determined using the criteria described in Section 2. (c) Cartilage damage was evaluated based on safranin O and toluidine blue staining according to the criteria described in Section 2. Data are presented as mean ± SEM; n = 9. $^*P < .05$, significantly different as indicated
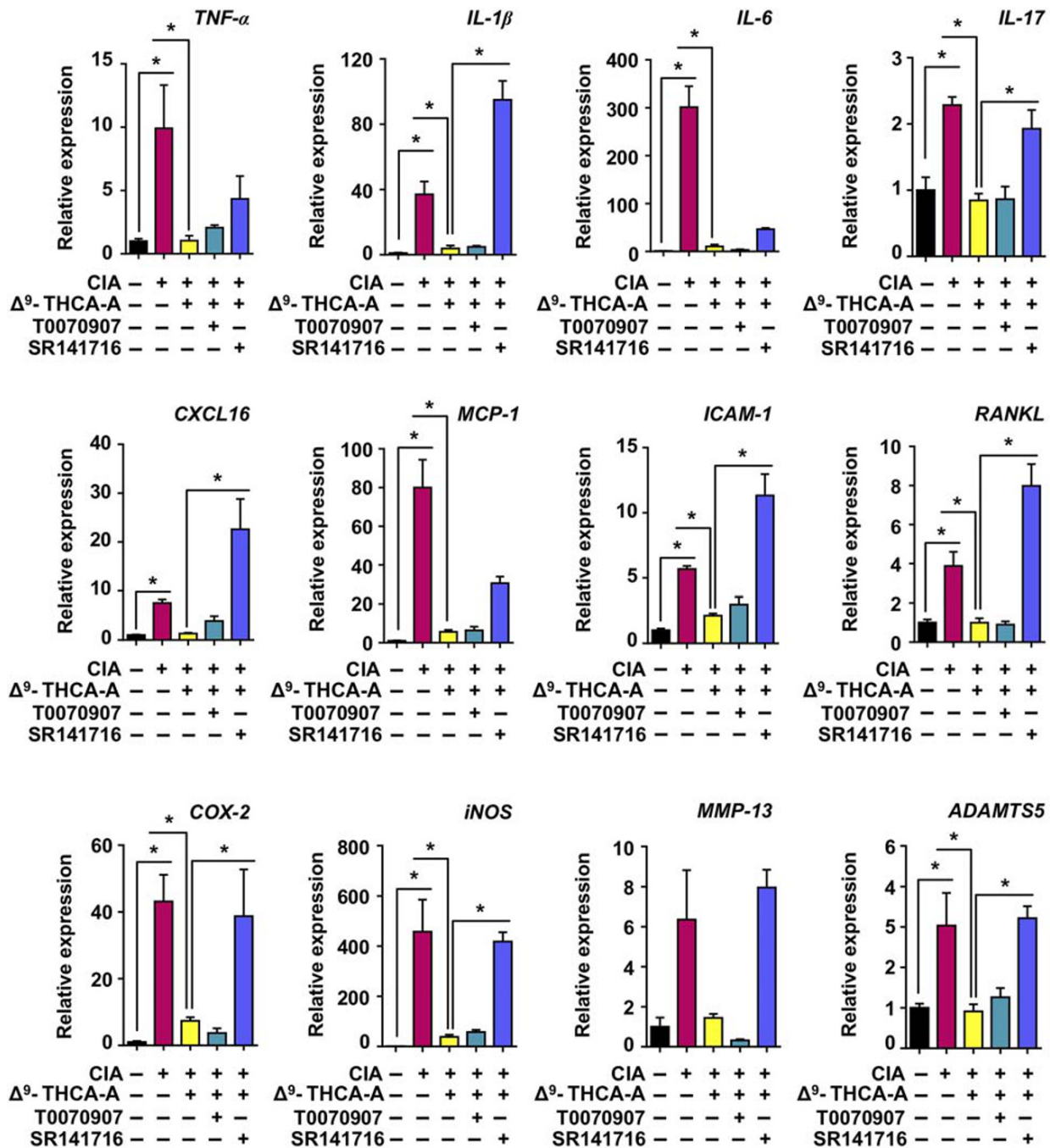
FIGURE 7 Effect of Δ^9-THCA-A on the gene expression of inflammatory/catabolic markers in knee joints. qPCR analysis of cytokines, proinflammatory mediators, and catabolic markers was performed on knee joints at the end of treatments. Results were obtained from nine mice per group and expressed as the mean ± SEM. $^*P < .05$, significantly different as indicated

Treatment with Δ^9-THCA-A significantly decreased the up-regulation of all the genes analysed (Figure 7). However, this inhibitory activity of Δ^9-THCA-A on proinflammatory gene expression was clearly blocked in most of the cases by SR141716 treatment but not by T0070907 treatment, thus suggesting that CB_1 receptors were the predominant targets for Δ^9-THCA-A at the articular level. Indeed, SR141716 treatment increased the expression of IL-1, ICAM-1, RANKL, and CXCL16.

3.4 | Effect of Δ^9-THCA-A on plasma biomarkers in CIA

CIA is an autoimmune disease, and peripheral markers also correlate with disease severity (Niu & Chen, 2014). Thus, we studied the plasma levels of proinflammatory cytokines and the presence of circulating anti-collagen antibodies at the end of treatment. The administration of CII caused a significant increase of IL-6 (Figure 8a), TNF-α
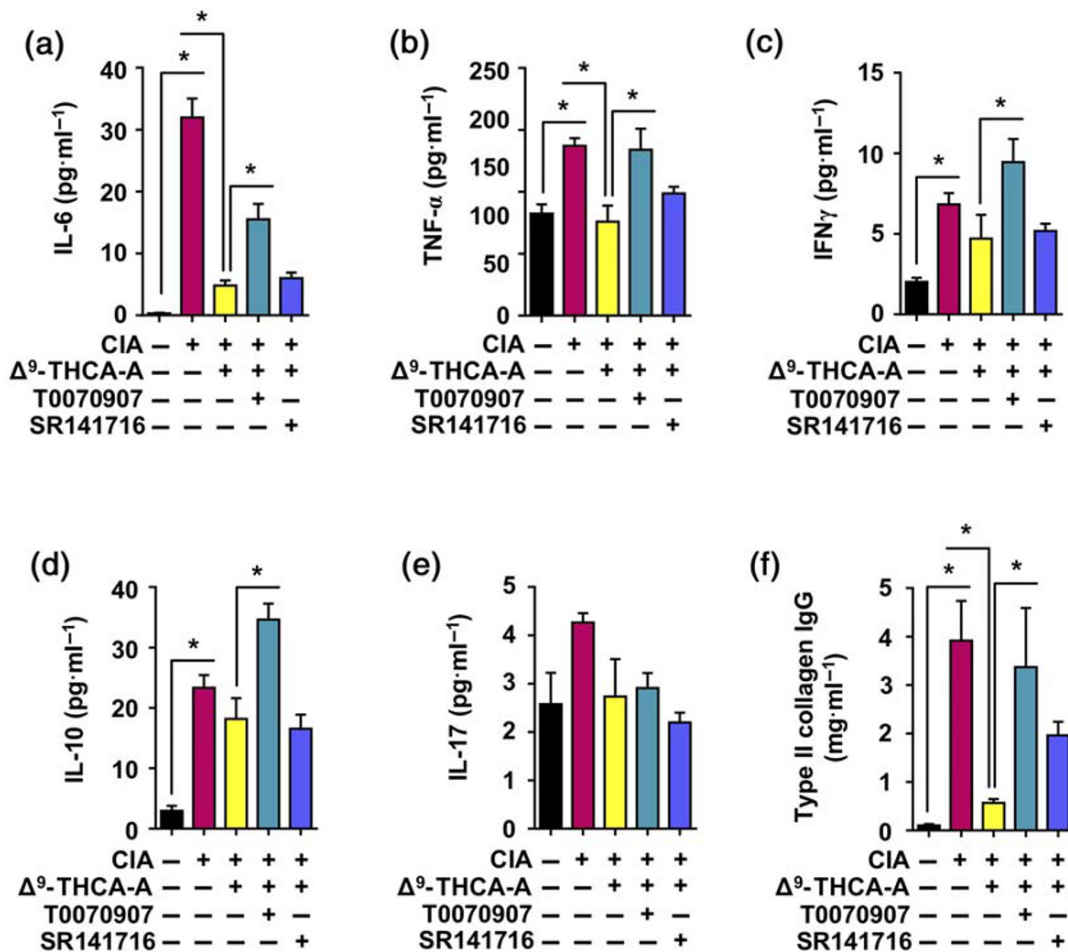
FIGURE 8 Effect of Δ^9-THCA-A on circulating profile of immunomodulatory cytokines in a mouse model of collagen-induced arthritis. A panel of cytokines was assayed in control and CIA mice by multiplex immunoassay at the end of the period of treatment. The cytokines assayed were (a) IL-6; (b) TNF-α; (c) IFN-γ; (d) IL-10; and (e) IL-17. In addition, (f) determination of total Ig antibodies against Type II Collagen by ELISA are shown for the five experimental groups. Values correspond to means ± SEM of nine mice per group. $^*P < 0.05$, significantly different as indicated

(Figure 8b), **IFN-γ** (Figure 8c), and **IL-10** levels (Figure 8d), together with a weak elevation of IL-17 levels (Figure 8e). Δ^9-THCA-A treatment fully normalized IL-6 and TNF-α levels and partly reduced IFN-γ, IL-17, and IL-10 concentrations. Notably, co-administration of T0070907 to Δ^9-THCA-A-treated CIA mice significantly increased IL-6, TNF-α, IFN-γ, and IL-10 levels. On the contrary, SR141716 only tended to increase the levels of TNF-α. To further confirm the anti-arthritic activity of Δ^9-THCA-A, we analysed the generation of anti-type II collagen antibody production, which plays a pathogenic role in CIA (Nandakumar et al., 2003). As shown in Figure 8f, Δ^9-THCA-A treatment significantly reduced plasma levels of type II collagen IgG relative to those in CIA group, whereas the treatment with T0070907 completely prevented that reduction and SR141716 trended to inhibit the Δ^9-THCA-A effect.

Finally, to complement the proteomic data, we investigated the plasma proteomic profile in mice to identify disease biomarkers that can be modified by Δ^9-THCA-A treatment. The analysis was performed by shotgun nLC-MS/MS followed by relative quantification by SWATH. In these experiments, albumin and immunoglobulins are removed before protein digestion, and so we cannot exclude the possibility that this process may also remove some cytokines and other proteins bound to albumin or to the column itself. Nevertheless, 346 proteins were identified and quantified. Comparisons of data from different conditions against controls revealed an interesting profile where, from the 28 proteins altered by CIA, 27 normalized their levels in response to the Δ^9-THCA-A treatment (adjusted $P < 0.1$ and absolute fold change >2). Furthermore, the combination of the Δ^9-THCA-A treatment with the antagonists of PPARγ or CB$_1$ receptors produced changes in 59 and 50 proteins, respectively, suggesting that the plasma proteomic profile is sensitive to the activity of both molecular targets (Figure 9a,b). Interestingly, from the 28 proteins mobilized by CIA, 22 were also altered when the Δ^9-THCA-A treatment was combined with any of the antagonists (Figure 9c). In this subset of 28 proteins, whose levels areshown in the Figure 9d heatmap, we could find some proteins related with the PPARγ signalling activity such as fatty acid binding proteins 1 and 3 (**Fabp1** and **Fabp3**) and the apolipoproteins a1 and c3 (Apoa1 and Apoc3). Finally, a group of inter-α-trypsin
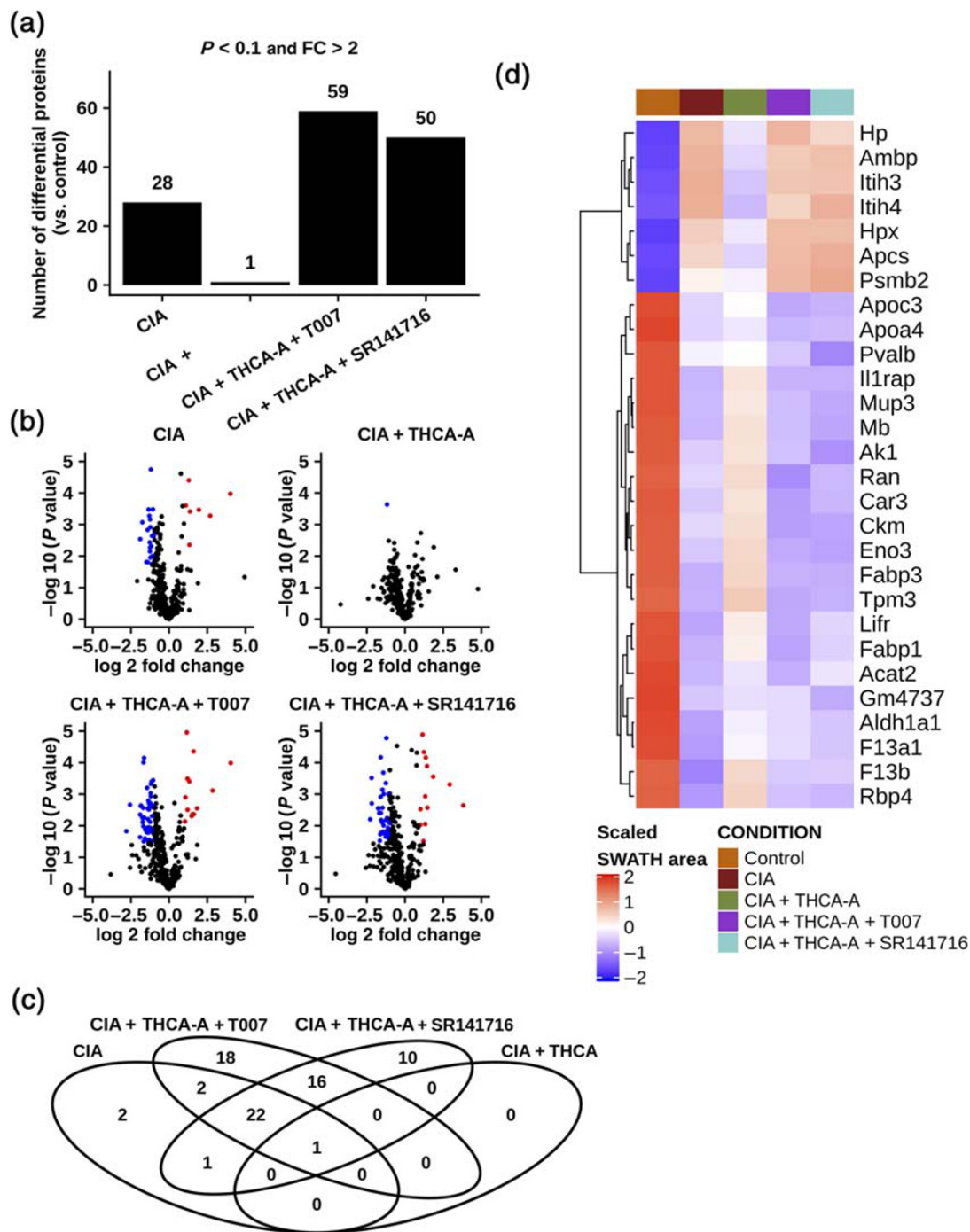
FIGURE 9 Proteomic analysis of Δ^9-THCA-A effects in plasma of CIA mice. (a) Bar plot reflecting the number of proteins that surpass the cut-off of an adjusted P value <0.1 and an absolute fold change >2 in every comparison. (b) Volcano plots showing the magnitude and significance of the changes by comparison. Each point represents a protein, and the colour indicates whether it is up-regulated (red) or down-regulated (blue), using the previously mentioned cut-off. (c) Venn diagram indicating the overlap between the groups of altered proteins. The red box highlights the 22 common for CIA, CIA + THCA + T0070907, and CIA + THCA + SR141716. (d) Heatmap depicting the abundance of the 28 significantly altered proteins in the CIA versus control comparison. The colour reflects the scaled normalized SWATH areas mean by group. Representative data from six mice per group are shown

inhibitors (Itih3, Itih4, and Ambp) increased their levels in CIA and were decreased with Δ^9-THCA-A treatment. The effect of Δ^9-THCA-A was also prevented in the presence of PPARγ or CB$_1$ receptor antagonists.

4 | DISCUSSION

We have previously reported that Δ^9-THCA-A binds and activates PPARγ and exerts potent anti-inflammatory activities in the CNS and

in peripherical inflammatory conditions (Nadal et al., 2017; Palomares et al., 2019). However, the biological activity of Δ^9-THCA-A through CB$_1$ receptors has been poorly investigated in vivo. In this study, we report for the first time that the non-psychotropic cannabinoid Δ^9-THCA-A modulates CB$_1$ receptors through the orthosteric and allosteric binding sites and shows efficacy as anti-arthritic treatment in mice through CB$_1$ receptor- and PPARγ-dependent pathways. Following CIA immunization, a Th1 cell response develops in the lymph nodes draining the site of challenge. Th1 cells then produce IFN-γ that acts as an isotype switch factor favouring the production of IgG2a by activated CII-specific B cells. Activated Th1 cells and IgG2a antibodies enter the joint triggering the activation of blood vessel endothelium and facilitating the early entry of autoreactive immune cells resulting finally in synovial inflammation and joint damage (Luross & Williams, 2001). Thus, it is possible that Δ^9-THCA-A may act at the articular level as well as the lymph nodes by inhibiting the autoimmune response to collagen. Nevertheless, the role of CB$_1$ receptor ligand agonists and antagonists in arthritis is intriguing. For instance, SR141716 alleviates CIA in obese but not in lean rats (Croci & Zarini, 2007). In addition, CB$_1$ receptor agonists and antagonists have shown a positive effect on arthritis inflammation (Lowin & Straub, 2015). These contradictory results can be explained by rapid desensitization and down-regulation of CB$_1$ receptors (Jin et al., 1999). Thus, the effect of Δ^9-THCA-A on CB$_1$ receptor desensitization and down-regulation or internalization through the orthosteric and allosteric sites required further research.

The multiple functions of the CB$_1$ receptor are due to a complex cellular signalling pathways that may depend on the structure of receptor complexes and the type of ligands. This functional selectivity is also known as biased agonism, and it has been postulated that CB$_1$ receptor-mediated signalling mediated by orthosteric ligands occurs in three different waves. The first wave is transient and mediated by heterotrimeric G-proteins that can dissociate the $\beta\gamma$ subunit and activate ERK1/2. After that, the second wave is mediated by β-arrestin recruitment that can also activate ERK1/2. The final wave is elicited either by G-protein or β-arrestins (Nogueras-Ortiz & Yudowski, 2016). Our in silico and in vitro results demonstrated that Δ^9-THCA-A can act as a functional orthosteric and also as a PAM of CB$_1$ receptors. For instance, both CP-55,940 and Δ^9-THCA-A induced ERK 1/2 phosphorylation, and this activity is blocked in the presence of SR141716 suggesting that Δ^9-THCA-A through the orthosteric side may activate this pathway via $\beta\gamma$ subunit dissociation. However, Δ^9-THCA-A did not activate the cAMP pathway nor induce β-arrestin recruitment but increased these activities induced by CP-55,940, confirming the PAM nature of Δ^9-THCA-A. In this sense, Δ^9-THCA-A may bind to the allosteric sites in CB$_1$ receptors when the orthosteric site is occupied by the endogenous CB$_1$ receptor ligand 2-AG (Figure S4). Although docking experiments strongly suggest that Δ^9-THCA-A may bind to specific allosteric sites, further experiments will be required to validate this finding. Our working hypothesis is that Δ^9-THCA-A, as well as its metabolite 11-OH-Δ^9-THCA-A (Figure S4), could bind to the orthosteric site of CB$_1$ receptors with lower affinity than full agonists and then can be displaced to the allosteric sites

when full agonists such as CP-55,940 and 2-AG are occupying the orthosteric site. Thus, Δ^9-THCA-A can act as PAM for CB$_1$ receptors in disease conditions where 2-AG levels are elevated. In this sense, elevated levels of 2-AG have been found in the synovial liquid of arthritis patients and in animal models (Richardson et al., 2008; Valastro et al., 2017). Accordingly, our data suggest that Δ^9-THCA-A could be maintaining the balance between the catabolic activities of MMPs and its inhibitors by acting as a PAM for CB$_1$ receptors and increasing the effect of endocannabinoids such as 2-AG (Dunn, Wilkinson, Crawford, Le Maitre, & Bunning, 2012). For instance, the inhibition of inflammatory cytokines such as IL-1β and TNF-α may prevent the expression of MMPs and aggrecanases by chondrocytes and inflammatory cells infiltrated in the synovium (Dunn et al., 2012). We also found that at the articular level, SR141716 treatment significantly increases the expression of IL-1β, ICAM-1, RANKL, and CXCL16 in CIA mice treated with Δ^9-THCA-A. However, this increase in these proinflammatory markers does not affect the therapeutic effect of Δ^9-THCA-A in CIA mice. Moreover, SR141716 alone did not show a therapeutic effect on CIA mice.

Although most of Δ^9-THCA-A action in joint inflammation and degeneration seems to be mediated through a CB$_1$ receptor-dependent pathway, we found that Δ^9-THCA-A also has anti-arthritis activity by acting through PPARγ. Here, we demonstrated that Δ^9-THCA-A showed a pattern of systemic protection, reducing the circulation of proinflammatory cytokines as well as the generation of anti-CII antibodies in CIA mice. These results suggest a potential peripheral role for Δ^9-THCA-A in regulating B and T cell response in lymph nodes that can be mediated through a PPARγ-dependent pathway.

Several studies have identified some potential plasma biomarkers as a reflection of pathological processes in RA patients (Niu & Chen, 2014). Furthermore, these biomarkers may be used to predict response to therapy and disease prognosis. Notably, one of the strengths of this study is the use of SWATH-MS as a tool for predicting Δ^9-THCA-A response in mice and perhaps in patients (Anjo, Santa, & Manadas, 2017). We identified 27 plasma proteins in CIA mice whose levels were totally reversed with Δ^9-THCA-A treatment through PPARγ and CB$_1$ receptor activation. Interestingly, our study revealed a preventive effect over inter-α-trypsin inhibitor heavy chain H3/4 (Itih3/Itih4) and proteasome subunit β type-2 (Pmbs2) whose increased concentration in sera of patients with RA was associated with disease activity and has been used as specific biomarkers (Kawaguchi et al., 2018; Liao et al., 2016). In addition, Δ^9-THCA-A treatment also prevented the secretion of acute-phase proteins, including haemopexin (Hpx) and haptoglobin (Hp), synthesized in response to a proinflammatory milieu (Baig et al., 2018; Park, Oh, Kim, Cho, & Kim, 2013). These proteins, as well as α-1-microglobulin/bikunin precursor (Ambp), are directly involved in the regulation of haem/iron metabolism (Olsson et al., 2012; Smith & McCulloh, 2015), which has been found to be frequently dysregulated in chronic inflammatory diseases such as RA (Baker & Ghio, 2009; Osterholm & Georgieff, 2015). Δ^9-THCA-A treatment also normalized the plasma levels of serum amyloid P component (Apcs) in CIA mice,

and elevated levels of Apcs have also been found in RA patients and in those who have amyloidosis associated with a rheumatic disease (Strachan & Johnson, 1982).

Finally, taken together, these results demonstrate that Δ^9-THCA-A is acting peripherally through CB_1 receptor and PPARγ signalling pathways. The lack of psychotropic activity of Δ^9-THCA-A may be explained by its binding mode to CB_1 receptors and the low CNS penetration of acidic cannabinoids (Anderson, Low, Banister, McGregor, & Arnold, 2019). A possible caveat of our study is that we cannot discard that a contamination with Δ^9-THC is mediating some of the effects observed in CIA mice and further experiments are required to exclude this possibility. Altogether, these features add to our current efforts to identify pharmacological agents capable to have anti-arthritis activity without undesired side effects and suggest that Δ^9-THCA-A, as well as non-decarboxylated *C. sativa* extracts, are worth considering for the management of rheumatic diseases and perhaps other inflammatory and autoimmune diseases.

AUTHOR CONTRIBUTIONS

B.P., G.M., and E.M. contributed to the conception and design of the study. B.P., C.G.C., M.G.C., and J.A.C. performed in vitro and in vivo experiments. B.P. and M.G.R. conducted the statistical analysis. C.G.C., M.G.C., and J.F.R. performed binding studies. S.S. and R.S. performed in silico analyses. M.G.R. and M.A.C. performed proteomic studies. B.P., G.A., and E.M. wrote and revised the manuscript. All the authors contributed to the analysis and interpretation of data and critically reviewed and approved the manuscript.

CONFLICT OF INTEREST

The authors declare no conflicts of interest.

DECLARATION OF TRANSPARENCY AND SCIENTIFIC RIGOUR

This Declaration acknowledges that this paper adheres to the principles for transparent reporting and scientific rigour of preclinical research as stated in the *BJP* guidelines for Design & Analysis, Immunoblotting and Immunochemistry, and Animal Experimentation, and as recommended by funding agencies, publishers, and other organizations engaged with supporting research.

ORCID

Javier Fernández-Ruiz [ID] https://orcid.org/0000-0002-4490-0604
Eduardo Muñoz [ID] https://orcid.org/0000-0001-8478-5842

REFERENCES

Alexander, S. P. H., Christopoulos, A., Davenport, A. P., Kelly, E., Mathie, A., Peters, J. A., … CGTP Collaborators. (2019). THE CONCISE GUIDE TO PHARMACOLOGY 2019/20: G protein-coupled receptors. *British Journal of Pharmacology*, *176*, S21–S141. https://doi.org/10.1111/bph.14748

Alexander, S. P. H., Cidlowski, J. A., Kelly, E., Mathie, A., Peters, J. A., Veale, E. L., … CGTP Collaborators. (2019). THE CONCISE GUIDE TO PHARMACOLOGY 2019/20: Nuclear hormone receptors. *British Journal of Pharmacology*, *176*, S229–S246. https://doi.org/10.1111/bph.14750

Alexander, S. P. H., Fabbro, D., Kelly, E., Mathie, A., Peters, J. A., Veale, E. L., … CGTP Collaborators. (2019). THE CONCISE GUIDE TO PHARMACOLOGY 2019/20: Enzymes. *British Journal of Pharmacology*, *176*, S297–S396. https://doi.org/10.1111/bph.14752

Alexander, S. P. H., Kelly, E., Mathie, A., Peters, J. A., Veale, E. L., Faccenda, E., … CGTP Collaborators. (2019). THE CONCISE GUIDE TO PHARMACOLOGY 2019/20: Other Protein Targets. *British Journal of Pharmacology*, *176*, S1–S20. https://doi.org/10.1111/bph.14747

Anderson, L. L., Low, I. K., Banister, S. D., McGregor, I. S., & Arnold, J. C. (2019). Pharmacokinetics of phytocannabinoid acids and anticonvulsant effect of cannabidiolic acid in a mouse model of Dravet syndrome. *Journal of Natural Products*, *82*, 3047–3055. https://doi.org/10.1021/acs.jnatprod.9b00600

Anjo, S. I., Santa, C., & Manadas, B. (2017). SWATH-MS as a tool for biomarker discovery: From basic research to clinical applications. *Proteomics*, *17*. https://doi.org/10.1002/pmic.201600278

Atilgan, A. R., Durell, S. R., Jernigan, R. L., Demirel, M. C., Keskin, O., & Bahar, I. (2001). Anisotropy of fluctuation dynamics of proteins with an elastic network model. *Biophysical Journal*, *80*, 505–515. https://doi.org/10.1016/S0006-3495(01)76033-X

Baig, S., Du, Y., Ling, Q., Paglicawan, L., Vanarsa, K., & Mohan, C. (2018). Hemopexin deficiency prevents joint injury following collagen antibody-induced arthritis. *The Journal of Inmunology*, *200*.

Baker, J. F., & Ghio, A. J. (2009). Iron homoeostasis in rheumatic disease. *Rheumatology (Oxford)*, *48*, 1339–1344. https://doi.org/10.1093/rheumatology/kep221

Bruni, N., Della Pepa, C., Oliaro-Bosso, S., Pessione, E., Gastaldi, D., & Dosio, F. (2018). Cannabinoid delivery systems for pain and inflammation treatment. *Molecules*, *23*. https://doi.org/10.3390/molecules23102478

Choi, Y. H., Hazekamp, A., Peltenburg-Looman, A. M., Frédérich, M., Erkelens, C., Lefeber, A. W., & Verpoorte, R. (2004). NMR assignments of the major cannabinoids and cannabiflavonoids isolated from flowers of Cannabis sativa. *Phytochem Anal.*, *15*, 345–354. https://doi.org/10.1002/pca.787

Croci, T., & Zarini, E. (2007). Effect of the cannabinoid CB1 receptor antagonist rimonabant on nociceptive responses and adjuvant-induced arthritis in obese and lean rats. *British Journal of Pharmacology*, *150*, 559–566. https://doi.org/10.1038/sj.bjp.0707138

Cuadari, A., Pollastro, F., Unciti-Broceta, J. D., Caprioglio, D., Minassi, A., Lopatriello, A., ... Appendino, G. (2019). The dimerization of Δ (9)-tetrahydrocannabinolic acid A (THCA-A). *Acta Pharm Sin B*, *9*, 1078–1083.

Curtis, M. J., Alexander, S., Cirino, G., Docherty, J. R., George, C. H., Giembycz, M. A., ... Ahluwalia, A. (2018). Experimental design and analysis and their reporting II: Updated and simplified guidance for authors and peer reviewers. *British Journal of Pharmacology*, *175*, 987–993. https://doi.org/10.1111/bph.14153

Dunn, S. L., Wilkinson, J. M., Crawford, A., Le Maitre, C. L., & Bunning, R. A. (2012). Cannabinoids: Novel therapies for arthritis? *Future Medicinal Chemistry*, *4*, 713–725. https://doi.org/10.4155/fmc.12.20

Fahmi, H., Martel-Pelletier, J., Pelletier, J. P., & Kapoor, M. (2011). Peroxisome proliferator-activated receptor gamma in osteoarthritis. *Modern Rheumatology*, *21*, 1–9. https://doi.org/10.3109/s10165-010-0347-x

Friesner, R. A., Banks, J. L., Murphy, R. B., Halgren, T. A., Klicic, J. J., Mainz, D. T., ... Shenkin, P. S. (2004). Glide: A new approach for rapid, accurate docking and scoring. 1. Method and assessment of docking accuracy. *Journal of Medicinal Chemistry*, *47*, 1739–1749. https://doi.org/10.1021/jm0306430

Friesner, R. A., Murphy, R. B., Repasky, M. P., Frye, L. L., Greenwood, J. R., Halgren, T. A., ... Mainz, D. T. (2006). Extra precision glide: Docking and scoring incorporating a model of hydrophobic enclosure for protein-ligand complexes. *Journal of Medicinal Chemistry*, *49*, 6177–6196. https://doi.org/10.1021/jm051256o

Gomez-Canas, M., Morales, P., Garcia-Toscano, L., Navarrete, C., Munoz, E., Jagerovic, N., et al. (2016). Biological characterization of PM226, a chromenoisoxazole, as a selective CB2 receptor agonist with neuroprotective profile. *Pharmacological Research*, *110*, 205–215. https://doi.org/10.1016/j.phrs.2016.03.021

Goncalves, J., Rosado, T., Soares, S., Simao, A. Y., Caramelo, D., Luis, A., et al. (2019). Cannabis and its secondary metabolites: Their use as therapeutic drugs, toxicological aspects, and analytical determination. *Medicines (Basel)*, *6*.

Grebner, C., Lecina, D., Gil, V., Ulander, J., Hansson, P., Dellsen, A., ... Guallar, V. (2017). Exploring binding mechanisms in nuclear hormone receptors by Monte Carlo and X-ray-derived motions. *Biophysical Journal*, *112*, 1147–1156. https://doi.org/10.1016/j.bpj.2017.02.004

Gui, H., Tong, Q., Qu, W., Mao, C. M., & Dai, S. M. (2015). The endocannabinoid system and its therapeutic implications in rheumatoid arthritis. *International Immunopharmacology*, *26*, 86–91. https://doi.org/10.1016/j.intimp.2015.03.006

Guo, Q., Wang, Y., Xu, D., Nossent, J., Pavlos, N. J., & Xu, J. (2018). Rheumatoid arthritis: Pathological mechanisms and modern pharmacologic therapies. *Bone Res*, *6*, 15. https://doi.org/10.1038/s41413-018-0016-9

Hanus, L. O., Meyer, S. M., Munoz, E., Taglialatela-Scafati, O., & Appendino, G. (2016). Phytocannabinoids: A unified critical inventory. *Natural Product Reports*, *33*, 1357–1392. https://doi.org/10.1039/C6NP00074F

Harding, S.D., Sharman, J.L., Faccenda, E., Southan, C., Pawson AJ, Ireland S, Gray AJG, Bruce L, Alexander SPH, Anderton S, Bryant C, Davenport AP, Doerig C, Fabbro D, Levi-Schaffer F, Spedding M, Davies JA, NC-IUPHAR (2018). The IUPHAR/BPS Guide to PHARMACOLOGY in 2018: updates and expansion to encompass the new guide to IMMUNOPHARMACOLOGY. *Nucleic Acids Res. 46*, D1091-1106. https://doi.org/10.1093/nar/gkx1121

Holmdahl, R., Jansson, L., Larsson, E., Rubin, K., & Klareskog, L. (1986). Homologous type II collagen induces chronic and progressive arthritis in mice. *Arthritis and Rheumatism*, *29*, 106–113. https://doi.org/10.1002/art.1780290114

Hua, T., Vemuri, K., Nikas, S. P., Laprairie, R. B., Wu, Y., Qu, L., ... Liu, Z. J. (2017). Crystal structures of agonist-bound human cannabinoid receptor CB1. *Nature*, *547*, 468–471. https://doi.org/10.1038/nature23272

Ignatowska-Jankowska, B. M., Baillie, G. L., Kinsey, S., Crowe, M., Ghosh, S., Owens, R. A., ... Ross, R. A. (2015). A cannabinoid CB1 receptor-positive allosteric modulator reduces neuropathic pain in the mouse with no psychoactive effects. *Neuropsychopharmacology*, *40*, 2948–2959. https://doi.org/10.1038/npp.2015.148

Jin, W., Brown, S., Roche, J. P., Hsieh, C., Celver, J. P., Kovoor, A., ... Mackie, K. (1999). Distinct domains of the CB1 cannabinoid receptor mediate desensitization and internalization. *The Journal of Neuroscience*, *19*, 3773–3780. https://doi.org/10.1523/JNEUROSCI.19-10-03773.1999

Jorgensen, W. L. (1998). OPLS force fields. *Encyclopedia of computational chemistry* (Vol. 3). New York: Wiley.

Kapur, A., Hurst, D. P., Fleischer, D., Whitnell, R., Thakur, G. A., Makriyannis, A., ... Abood, M. E. (2007). Mutation studies of Ser7.39 and Ser2.60 in the human CB1 cannabinoid receptor: Evidence for a serine-induced bend in CB1 transmembrane helix 7. *Molecular Pharmacology*, *71*, 1512–1524. https://doi.org/10.1124/mol.107.034645

Kawaguchi, H., Matsumoto, I., Osada, A., Kurata, I., Ebe, H., Tanaka, Y., ... Sumida, T. (2018). Identification of novel biomarker as citrullinated inter-alpha-trypsin inhibitor heavy chain 4, specifically increased in sera with experimental and rheumatoid arthritis. *Arthritis Research & Therapy*, *20*, 66. https://doi.org/10.1186/s13075-018-1562-7

Kilkenny, C., Browne, W. J., Cuthill, I. C., Emerson, M., & Altman, D. G. (2010). Improving bioscience research reporting: The ARRIVE guidelines for reporting animal research. *PLoS Biology*, *8*, e1000412. https://doi.org/10.1371/journal.pbio.1000412

Koufany, M., Chappard, D., Netter, P., Bastien, C., Weryha, G., Jouzeau, J. Y., & Moulin, D. (2013). The peroxisome proliferator-activated receptor γ agonist pioglitazone preserves bone microarchitecture in experimental arthritis by reducing the interleukin-17-dependent osteoclastogenic pathway. *Arthritis and Rheumatism*, *65*, 3084–3095. https://doi.org/10.1002/art.38130

Kraus, J. (2012). Expression and functions of μ-opioid receptors and cannabinoid receptors type 1 in T lymphocytes. *Annals of the New York Academy of Sciences*, *1261*, 1–6. https://doi.org/10.1111/j.1749-6632.2012.06524.x

Krejci, Z. D., & Santavy, F. (1955). Isolace dalších látek z listí indického konopí Cannabis sativa L. [Isolation of other substances from the leaves of the Indian hemp (Cannabis sativa L., varietas indica.)]. *Acta Universitatis Palackianae Olumucensis*, *VI*, 59–66.

Krejci, Z., Horak, M., & Santavy, F. (1959). Hemp (*Cannabis sativa*)—An antibiotic drug. 3. Isolation and constitution of two acids from *Cannabis sativa*. *Die Pharmazie*, *14*, 349–355.

Krishna Kumar, K., Shalev-Benami, M., Robertson, M. J., Hu, H., Banister, S. D., Hollingsworth, S. A., et al. (2019). Structure of a signaling cannabinoid receptor 1-G protein complex. *Cell*, *176*(448–458), e412.

Lecina, D., Gilabert, J. F., & Guallar, V. (2017). Adaptive simulations, towards interactive protein-ligand modeling. *Scientific Reports*, *7*, 8466. https://doi.org/10.1038/s41598-017-08445-5

Liao, C. C., Chou, P. L., Cheng, C. W., Chang, Y. S., Chi, W. M., Tsai, K. L., ... Lin, C. Y. (2016). Comparative analysis of novel autoantibody isotypes against citrullinated-inter-alpha-trypsin inhibitor heavy chain 3 (ITIH3) (542-556) peptide in serum from Taiwanese females with rheumatoid arthritis, primary Sjogren's syndrome and secondary Sjogren's syndrome in rheumatoid arthritis. *Journal of Proteomics*, *141*, 1–11. https://doi.org/10.1016/j.jprot.2016.03.031

Lowin, T., & Straub, R. H. (2015). Cannabinoid-based drugs targeting CB1 and TRPV1, the sympathetic nervous system, and arthritis.

Arthritis Research & Therapy, *17*, 226. https://doi.org/10.1186/s13075-015-0743-x

Luross, J. A., & Williams, N. A. (2001). The genetic and immunopathological processes underlying collagen-induced arthritis. *Immunology*, *103*, 407–416. https://doi.org/10.1046/j.1365-2567.2001.01267.x

Marder, W., Khalatbari, S., Myles, J. D., Hench, R., Lustig, S., Yalavarthi, S., et al. (2013). The peroxisome proliferator activated receptor-γ pioglitazone improves vascular function and decreases disease activity in patients with rheumatoid arthritis. *Journal of the American Heart Association*, *2*, e000441.

McInnes, I. B., & Schett, G. (2011). The pathogenesis of rheumatoid arthritis. *The New England Journal of Medicine*, *365*, 2205–2219. https://doi.org/10.1056/NEJMra1004965

McPartland, J. M., MacDonald, C., Young, M., Grant, P. S., Furkert, D. P., & Glass, M. (2017). Affinity and efficacy studies of tetrahydrocannabinolic acid A at cannabinoid receptor types one and two. *Cannabis Cannabinoid Res*, *2*, 87–95. https://doi.org/10.1089/can.2016.0032

Mella, R. M., Kortazar, D., Roura-Ferrer, M., Salado, C., Valcarcel, M., Castilla, A., et al. (2018). Nomad biosensors: A new multiplexed technology for the screening of GPCR ligands. *SLAS Technol*, *23*, 207–216. https://doi.org/10.1177/2472630318754828

Moreno-Sanz, G. (2016). Can you pass the acid test? Critical review and novel therapeutic perspectives of Δ^9-tetrahydrocannabinolic acid A. *Cannabis Cannabinoid Res*, *1*, 124–130. https://doi.org/10.1089/can.2016.0008

Nadal, X., Del Rio, C., Casano, S., Palomares, B., Ferreiro-Vera, C., Navarrete, C., et al. (2017). Tetrahydrocannabinolic acid is a potent PPARγ agonist with neuroprotective activity. *British Journal of Pharmacology*, *174*, 4263–4276. https://doi.org/10.1111/bph.14019

Nandakumar, K. S., Andren, M., Martinsson, P., Bajtner, E., Hellstrom, S., Holmdahl, R., et al. (2003). Induction of arthritis by single monoclonal IgG anti-collagen type II antibodies and enhancement of arthritis in mice lacking inhibitory FcγRIIB. *European Journal of Immunology*, *33*, 2269–2277. https://doi.org/10.1002/eji.200323810

Niu, X., & Chen, G. (2014). Clinical biomarkers and pathogenic-related cytokines in rheumatoid arthritis. *Journal of Immunology Research*, *2014*, 698192.

Nogueras-Ortiz, C., & Yudowski, G. A. (2016). The multiple waves of cannabinoid 1 receptor signaling. *Molecular Pharmacology*, *90*, 620–626. https://doi.org/10.1124/mol.116.104539

Olsson, M. G., Allhorn, M., Bulow, L., Hansson, S. R., Ley, D., Olsson, M. L., et al. (2012). Pathological conditions involving extracellular hemoglobin: Molecular mechanisms, clinical significance, and novel therapeutic opportunities for α_1-microglobulin. *Antioxidants & Redox Signaling*, *17*, 813–846. https://doi.org/10.1089/ars.2011.4282

Onufriev, A., Bashford, D., & Case, D. A. (2004). Exploring protein native states and large-scale conformational changes with a modified generalized born model. *Proteins*, *55*, 383–394. https://doi.org/10.1002/prot.20033

Ormseth, M. J., Oeser, A. M., Cunningham, A., Bian, A., Shintani, A., Solus, J., ... Stein, C. (2013). Peroxisome proliferator-activated receptor γ agonist effect on rheumatoid arthritis: A randomized controlled trial. *Arthritis Research & Therapy*, *15*, R110. https://doi.org/10.1186/ar4290

Ortea, I., Ruiz-Sanchez, I., Canete, R., Caballero-Villarraso, J., & Canete, M. D. (2018). Identification of candidate serum biomarkers of childhood-onset growth hormone deficiency using SWATH-MS and feature selection. *Journal of Proteomics*, *175*, 105–113. https://doi.org/10.1016/j.jprot.2018.01.003

Osterholm, E. A., & Georgieff, M. K. (2015). Chronic inflammation and iron metabolism. *The Journal of Pediatrics*, *166*(1351–1357), e1351.

Palomares, B., Ruiz-Pino, F., Garrido-Rodriguez, M., Eugenia Prados, M., Sanchez-Garrido, M. A., Velasco, I., et al. (2019). Tetrahydrocannabinolic acid A (THCA-A) reduces adiposity and prevents metabolic disease caused by diet-induced obesity. *Biochemical Pharmacology*, *171*, 113693.

Pandey, P., Roy, K., Liu, H., Ma, G., & Pettaway, S. (2018). Structure-based identification of potent natural product chemotypes as cannabinoid receptor 1 inverse agonists. *Molecules*, *23*(10), 2630. https://doi.org/10.3390/molecules23102630

Park, H. J., Oh, M. K., Kim, N. H., Cho, M. L., & Kim, I. S. (2013). Identification of a specific haptoglobin C-terminal fragment in arthritic synovial fluid and its effect on interleukin-6 expression. *Immunology*, *140*, 133–141. https://doi.org/10.1111/imm.12125

Richardson, D., Pearson, R. G., Kurian, N., Latif, M. L., Garle, M. J., Barrett, D. A., ... Chapman, V. (2008). Characterisation of the cannabinoid receptor system in synovial tissue and fluid in patients with osteoarthritis and rheumatoid arthritis. *Arthritis Research & Therapy*, *10*, R43. https://doi.org/10.1186/ar2401

Rock, E. M., Kopstick, R. L., Limebeer, C. L., & Parker, L. A. (2013). Tetrahydrocannabinolic acid reduces nausea-induced conditioned gaping in rats and vomiting in *Suncus murinus*. *British Journal of Pharmacology*, *170*, 641–648. https://doi.org/10.1111/bph.12316

Seeuws, S., Jacques, P., Van Praet, J., Drennan, M., Coudenys, J., Decruy, T., et al. (2010). A multiparameter approach to monitor disease activity in collagen-induced arthritis. *Arthritis Research & Therapy*, *12*, R160. https://doi.org/10.1186/ar3119

Shao, Z., Yan, W., Chapman, K., Ramesh, K., Ferrell, A. J., Yin, J., ... Rosenbaum, D. M. (2019). Structure of an allosteric modulator bound to the CB1 cannabinoid receptor. *Nature Chemical Biology*, *15*, 1199–1205. https://doi.org/10.1038/s41589-019-0387-2

Shim, J. Y., Bertalovitz, A. C., & Kendall, D. A. (2011). Identification of essential cannabinoid-binding domains: Structural insights into early dynamic events in receptor activation. *The Journal of Biological Chemistry*, *286*, 33422–33435. https://doi.org/10.1074/jbc.M111.261651

Slivicki, R. A., Xu, Z., Kulkarni, P. M., Pertwee, R. G., Mackie, K., Thakur, G. A., & Hohmann, A. G. (2018). Positive allosteric modulation of cannabinoid receptor type 1 suppresses pathological pain without producing tolerance or dependence. *Biological Psychiatry*, *84*, 722–733. https://doi.org/10.1016/j.biopsych.2017.06.032

Smith, A., & McCulloh, R. J. (2015). Hemopexin and haptoglobin: Allies against heme toxicity from hemoglobin not contenders. *Frontiers in Physiology*, *6*, 187.

Strachan, A. F., & Johnson, P. M. (1982). Protein SAP (serum amyloid P-component) in Waldenstrom's macroglobulinaemia, multiple myeloma and rheumatic diseases. *Journal of Clinical & Laboratory Immunology*, *8*, 153–156.

Szanto, A., & Nagy, L. (2008). The many faces of PPARγ: Anti-inflammatory by any means? *Immunobiology*, *213*, 789–803. https://doi.org/10.1016/j.imbio.2008.07.015

Tam, J., Trembovler, V., Di Marzo, V., Petrosino, S., Leo, G., Alexandrovich, A., et al. (2008). The cannabinoid CB1 receptor regulates bone formation by modulating adrenergic signaling. *FASEB Journal: Official Publication of the Federation of American Societies for Experimental Biology*, *22*, 285–294. https://doi.org/10.1096/fj.06-7957com

Valastro, C., Campanile, D., Marinaro, M., Franchini, D., Piscitelli, F., Verde, R., ... di Bello, A. (2017). Characterization of endocannabinoids and related acylethanolamides in the synovial fluid of dogs with osteoarthritis: A pilot study. *BMC Veterinary Research*, *13*, 309. https://doi.org/10.1186/s12917-017-1245-7

Wang, M., Wang, Y. H., Avula, B., Radwan, M. M., Wanas, A. S., van Antwerp, J., ... Khan, I. A. (2016). Decarboxylation study of acidic cannabinoids: A novel approach using ultra-high-performance

supercritical fluid chromatography/photodiode array-mass spectrometry. *Cannabis Cannabinoid Res*, *1*, 262–271. https://doi.org/10.1089/can.2016.0020

SUPPORTING INFORMATION

Additional supporting information may be found online in the Supporting Information section at the end of this article.